Part II

Minimising statistical errors in gate calibration

Probabilities are intrinsic in quantum mechanics. Indeed, the theory of quantum mechanics states with which probability a concrete outcome of a measurement is obtained, but cannot predict the value of the outcome with certainty. As a direct consequence, a quantum experimentalist needs to carry out several runs of the same experiment. Then, a statistical treatment of the collected data should be conducted to estimate the measured quantities. This fact creates a dialogue between the disciplines of quantum mechanics and statistical theory, a dialogue that we will explore in this part of the thesis.

The second part of this thesis has two chapters. Within Chapter 3, we introduce the notions of statistics and gate calibration that are fundamental for our findings in Chapter 4.

Chapter 4 builds on the work presented in Ref. [39] about calibration of quantum-gate sets. In their work, a protocol called Gate Set Calibration protocol (GSC) is introduced and used to extract systematic gate errors. Although in quantum mechanics physical measurements have an intrinsic uncertainty, statistical errors are not considered in Ref. [39]. In this thesis, we conduct a statistical analysis of GSC in order to optimise the protocol. Not only is our goal to minimise statistical errors, but also to require physical realisability of GSC. For the latter, we restrict the implementation of GSC to involve a small number of different quantum gates as well as a small sequence length.

Chapter 3

Foundations

The first chapter of this part contains the theoretical foundations behind the research presented in Chapter 4. In Section 3.1, we review concepts about statistical theory. We start in Section 3.1.1 brushing up notions of multivariate probability distributions, such as random vector and the central limit theorem. We focus on the probability distributions that will be used in Chapter 4, namely the multivariate Gaussian distribution and the multivariate binomial distribution.

Section 3.1.2 is an introduction to the theory of design of experiments. After beginning with a general definition of the concept 'process', we review the goals of this theory. We then put the focus on nuisance factors, which are the factors with which we deal in Chapter 4.

To finish this chapter, we give a brief overview of the field of gate calibration in Sec. 3.2. Tomography protocols, as well as randomized benchmarking protocols, are explained. We also identify the scenarios where each calibration approach is more suitable.

3.1 Statistics

Within this section, we introduce basic notions of statistics that are essential for a clear understanding of the research presented in Chapter 4. Section 3.1.1 is about the branch of statistics that considers scenarios with more than one random variable. Afterwards, we explain the foundations of the branch of statistics called design of experiments.

3.1.1 Multivariate probability distributions

Many interesting problems in physics take place in a multidimensional space and involve vectors whose coordinates are correlated. A statistical analysis of these problems requires to deal with random variables which form a vector. Here, we review the basic notions of the branch of statistics that considers more than one random variable and constructs multivariate models. Along this section we will assume that random variables are continuous unless stated differently.

Consider k scalar-valued random variables, $X_1, \ldots, X_k$, on the same probability space with probability density functions $p(x_i)$ for all $i = 1, \ldots, k$. A *multivariate random vector* (or simply *random vector*), $\vec{X}$, is a k-dimensional vector with random variables as components, i.e., $\vec{X} = (X_1, \ldots, X_k)$.

A random vector gives rise to a *multivariate probability density function*, $p(x_1, \ldots, x_k)$, defined as the joint probability density function of all components of the random vector. Then, we write the joint probability of finding each random variable, X_i, in a concrete interval, $[a_i, b_i]$, as

$$\Pr[a_1 \leq X_1 \leq b_1 \text{ and } \ldots \text{ and } a_k \leq X_k \leq b_k] = \int_{a_1}^{b_1} \cdots \int_{a_k}^{b_k} p(x_1, \ldots, x_k) dx_1 \cdots dx_k,$$

which, by definition, satisfies

$$\int_{x_1} \cdots \int_{x_k} p(x_1, \ldots, x_k) dx_1 \cdots dx_k = 1.$$

The probability density functions of each component of the random vector, $p(x_i)$, are known as *marginal probability density functions*.

Analogously to univariate probability distributions, multivariate probability distributions are often parametrized by a couple of quantities with a practical interpretation. The *mean vector* of a random vector, $\vec{X}$, is $\mathrm{E}[\vec{X}] = (\mathrm{E}[X_1], \ldots, \mathrm{E}[X_k])$, which we will also sometimes denote as $\vec{\mu}$. The correlation between the random variables that form a random vector is specified with a matrix called *covariance matrix*. The covariance matrix, Σ, of a random vector, $\vec{X} = (X_1, \ldots, X_k)$, is a $k \times k$ matrix with entries

$$\Sigma_{ij} = \mathrm{cov}(X_i, X_j) = \mathrm{E}[(X_i - \mathrm{E}[X_i])(X_j - \mathrm{E}[X_j])] = \mathrm{E}[X_i X_j] - \mathrm{E}[X_j]\mathrm{E}[X_j].$$

Note that the diagonal entries of Σ are the variances of the random variables X_i.

When the random variables X_i are independent, the multivariate probability density function factorises and can be written as $p(x_1, \ldots, x_k) = p(x_1) \cdots p(x_k)$. Furthermore, in this case the covariance matrix is diagonal.

An important probability distribution is the Gaussian distribution, which can be extended to the multivariate case straightforwardly. Given a k-dimensional random vector, $\vec{X}$, it is said that $\vec{X}$ is distributed according to a *multivariate Gaussian distribution* if any linear combination of its k components is distributed according to a (univariate) Gaussian distribution. We write $\vec{X} \sim \mathcal{N}(\vec{\mu}, \Sigma)$, where $\vec{\mu}$ and Σ are the mean vector and the covariance matrix of $\vec{X}$, respectively.

The relevance of the (multivariate) Gaussian distribution comes from the well-known (multivariate) *Central Limit Theorem* (CLT). This theorem states that the mean value of many independent samples of a random vector, with finite mean and covariance matrix, is also a random vector. Furthermore, its probability distribution converges to a (multivariate) Gaussian distribution in the limit of a large number of samples.

Because of the CLT, the Gaussian distribution appears in many processes in nature that depend on multiple factors, such as neural activity, gene expression or measurement errors.

In quantum physics, the so-called binomial distribution, a discrete probability distribution, is also crucial since it appears in the context of quantum measurements. Consider an observable, $\hat{A}$, with two outcomes, a_1 and a_2, and an experimental setting that requires N measurements of the observable A. The data obtained in the experiment is distributed according to a binomial distribution. Specifically, the amount of times the measurement device returns the outcome a_i gives rise to a binomial distribution such that $B(N, p_i)$, where p_i is the probability of obtaining the outcome a_i. In the limit of large N, the binomial distribution can be approximated by a Gaussian distribution with parameters $\mathcal{N}(Np_i, Np_i(1-p_i))$ due to CLT.

When each random variable that constitutes a random vector gives rise to a (univariate) binomial distribution, we say that the random vector is distributed according to a *multivariate binomial distribution*.

Random vectors can be part of algebraic transformations during statistical analysis and create new vectors. A vector $\vec{Y} = M\vec{X} + \vec{v}$ is also a $k-$dimensional random vector if it is an affine transformation of the random vector $\vec{X}$, where M is a $k \times k$ matrix and $\vec{v}$ is a k-dimensional vector [40].

In the particular case that the random vector $\vec{X}$ is distributed according to a multivariate Gaussian distribution such that $\vec{X} \sim \mathcal{N}(\vec{\mu}, \Sigma)$, then the random vector $\vec{Y}$ also gives rise to a multivariate Gaussian distribution with mean vector $M\vec{\mu} + \vec{v}$, and covariance matrix $M\Sigma M^T$, i.e., $\vec{Y} \sim \mathcal{N}(M\vec{\mu} + \vec{v}, M\Sigma M^T)$.

Affine transformations of multivariate Gaussian distributions will be a crucial tool to improve the design of a calibration protocol in Ch. 4, but, first, we need to learn about design of experiments.

3.1.2 Design of experiments

Experimentation is required not only in science but also in industry and engineering. The efficiency of such experiments can benefit from statistical theory to obtain more robust and precise conclusions. Applying statistical theory to experimentation consists in planning an experiment to collect the appropriated data, and conducting statistical analysis to extract valid

and objective conclusions from the data. Therefore, there are two stages where statistics play a crucial role in any experiment: the design of the experiment and the statistical analysis of the collected data. This section is devoted to the former: the design of experiments (DOE). The material presented here is based on Ref. [41].

Consider a system in some initial conditions that undergoes a *process*. Figure 3.1 is a schematic description of a general process, where the initial conditions are referred to as *input variables*. The word process here refers to any transformation, including operations from industrial processing, such as changes caused by machines, or from quantum computing, such as applications of quantum gates and measurements. Two different kind of factors affect the process: the *controllable* and the *uncontrollable* factors. As their name suggests, the latter are caused by variables that one cannot modify, while the former can be adjusted. The process transforms the input into an *output* characterised by one or more response variables.

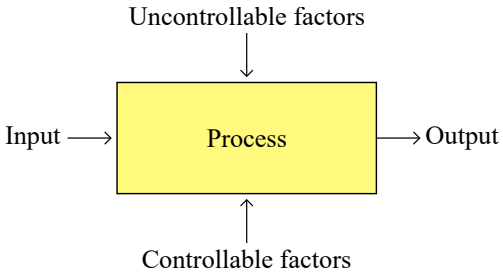

Figure 3.1: Schematic description of a process.

An *experiment* can be defined as a series of runs of a process. Thus, the output of an experiment is usually a data set.

In order to improve a process, DOE suggests to carry out experiments with the following goals:

1. Determining the most influential factors on the output,
2. Determining how to adjust the controllable factors such that the output's response variables are always near the desired value,
3. Determining how to adjust the controllable factors such that the variability of the response variables is small,
4. Determining how to adjust the controllable factors such that the effect of the uncontrollable factors is minimal.

We focus in this thesis on the last two goals of DOE. In particular, we put attention on the branch of DOE that takes care of *nuisance factors*, i.e., factors whose effect on the

output is significant enough to be considered even if we are not interested in their influence. Nuisance factors are classified as *controllable*, *uncontrollable* and *noise factors*. Controllable and uncontrollable nuisance factors can be measured. Moreover, the former can be adjusted and thus blocked, while the latter cannot be modified, so they need to be addressed with statistical analysis. A nuisance factor is called a noise factor when it is uncontrollable and varies naturally in each run of the process. This variability makes it impossible to control a noise factor only with one run of the process, but it might be addressed at the experiment level (i.e., doing several runs of a process). Noise factors are often managed by setting the controllable (design) factors of the process in a range that minimises the variability of the output responses.

Consider as an example the scenario that we study in Chapter 4: calibrating a quantum gate called CNOT. As devices are not perfect, the application of a CNOT is affected by uncontrollable nuisance factors and, instead of a CNOT gate, a perturbed version of the gate is applied. To account for these uncontrollable nuisance factors, we build a model for the perturbed gate that considers error parameters. Noise factors are also present in the calibration process due to quantum measurements. The output of a quantum measurement is a random variable, and thus it induces statistical errors. This statistical error is a noise factor because it cannot be controlled in a single process, and it varies in each run. However, we can reduce the statistical error by realising many runs of the process and, as we show in Chapter 4, by adjusting controllable factors of the calibration process. Before delving into the application of DOE on a gate calibration protocol, we review basic concepts of gate calibration in the next section.

3.2 Gate calibration

Theoretically, a quantum computation is a unitary matrix performed on a vector. In a laboratory, however, everything becomes messy. The vector corresponds to a physical system, which can spontaneously change its state due to undesired interactions with the environment. The unitary matrix corresponds to a series of pulses that must be precisely selected and performed to obtain the expected result. In order to consider all these factors, a model that characterises the quantum computation is designed. Then, experiments are carried out, and the data obtained is studied to choose the optimal values for the model parameters. This process is known as gate calibration and is indispensable in quantum computing. Within this section, we give an overview of gate calibration.

To design suitable gate calibration protocols, one must consider that errors in a quantum computer can have different origins. We can distinguish between coherent errors and incoherent errors. The former occur in the devices, while the latter arise from the interaction between

quantum systems and the environment. In order to have a quantum computer that applies operations close to the ideal unitary gates, both types of errors, incoherent and coherent, must be small enough [42, 43].

Maybe the most intuitive gate calibration strategy consists of fully characterising the quantum process, including its errors. Quantum process tomography (QPT) [44] and Gate Set Tomography (GST) [45] are the two most well-known methods to realise this task. QPT characterises a collection of states on which the process of interest has been applied, and uses this information to learn about the process. The characterisation of the resulting states is done via quantum state tomography [46, 47], which reconstructs a quantum state by performing measurements on a collection of identical states. QPT runs, however, into a self-consistency problem since it needs fiducial measurements and initial states, which, in turn, require already calibrated quantum gates.

The self-consistency problem of QPT can be solved using GST. GST has a similar spirit to QPT but includes State-Preparation and Measurement (SPAM) errors in its error model. Tomography methods provide a complete characterisation of the quantum process and can distinguish between individual gate errors and errors on the global gate set. Nevertheless, they are infeasible for large system sizes, since the number of measurements scales exponentially with the number of qubits.

To overcome the lack of scalability of tomography methods, calibration techniques that work with a partial characterisation of the quantum process, such as Randomized Benchmarking (RB) protocols, are used. Nowadays, RB refers to a family of calibration protocols [48, 49, 50, 51, 52, 53, 54, 55] based on the original proposal by Dankert et al. [56]. The idea behind these protocols consists of three steps. First, preparing an input state, then applying a squences of random gates, and finally measuring the resulting state. These three steps are repeated using sequences of different lengths. While errors in the gates are amplified with increasing sequence length, SPAM errors are independent of the sequence length. Moreover, the measured quantities only depend linearly on SPAM errors. These differences on the dependencies allow extracting an average error rate of the quantum process disentangled from SPAM errors by exponentially fitting the measured quantities versus the sequence length. RB protocols have been used widely because of their apparent advantages: scalability and easy implementation. Nevertheless, RB protocols are unsuitable for experiments requiring a detailed characterisation of individual quantum operations or distinguishing between incoherent and coherent errors.

Further calibration methods make use of ideas from both GST and RB [57, 58]. RB tomography [59], randomised linear GST [60] and compressive GST [61] are, for example,

calibration protocols that work on a trade-off between the information extracted from the quantum process and the resource requirements.

Another example of a calibration protocol that is a middle way between GST and RB is GSC, a protocol introduced in Ref. [39]. Given a set of available quantum gates, initial states and measurements, GSC constructs short gate sequences that allow all coherent gate errors to be extracted by solving an inverse problem. This protocol offers the flexibility to either be self-consistent or simplified for scenarios where single-qubit gates are already calibrated. Within Chapter 4, we review GSC in detail, and we apply the statistical theory presented in Sec. 3.1 to improve the design of this calibration protocol.

Chapter 4

Results

A fundamental property of quantum mechanics is its intrinsic uncertainty: responses of measurements can only be predicted probabilistically. Therefore, experiments aimed to extract information from a quantum system have to be designed so as to reduce the expected statistical uncertainty. The branch of statistics concerned with such questions is the Design of Experiments (DOE). Among the main objectives of DOE is the optimisation of statistical error, as well as validity, reliability and replicability. DOE has been applied in different quantum information problems such as parameter estimation [62, 63], and quantum state and process tomography [64, 65, 66]. In this chapter, we address the task of implementing DOE in a calibration protocol for quantum gate sets.

Specifically, we will work with the Gate Set Calibration protocol (GSC) introduced in Ref. [39] for the purpose of identifying coherent errors in unitary quantum gates. Given a set of available quantum gates, initial states and measurements, GSC constructs short gate sequences that allow all coherent gate errors to be extracted. This protocol can be considered as a middle way between randomized benchmarking and gate set tomography, as it provides more detailed information than the former using fewer measurements than the latter [50, 67].

In order to optimise GSC, we introduce parameters in the sequences that GSC builds and perform an optimisation over these parameters to minimise the statistical error of GSC.

This chapter is structured as follows. In Sec. 4.1, a simplified version of GSC is introduced and the notation is established. In Sec. 4.2 we present the theoretical framework under which the optimisation of GSC will be conducted. We analyse the statistics of GSC and define a measure of uncertainty that will allow us to compare the statistical error of different versions of GSC. Section 4.3 is dedicated to the optimisation of GSC by minimising the statistical error with respect to the measure of uncertainty. The version of GSC resulting from the optimisation is further modified to take into account the feasibility of the protocol. We verify in Sec. 4.3.1 that the reduction of the statistical error also holds when imperfect measurements are considered. An outlook is presented in Sec. 4.4. Note that this chapter has its own appendix.

4.1 The gate set calibration protocol

In Ref. [39], a new protocol for characterising and calibrating quantum gates, the GSC, has been introduced. This section will introduce the precise notation and present a slightly simplified version of the protocol. In particular, we restrict attention to the specific case of calibrating a two-qubit CNOT gate subject to coherent errors.

The GSC consists of the following steps. First, the qubits are initialised in a known state. Then, a gate sequence from a set of available gates is applied to the initial state, and finally, a measurement is performed. All coherent gate errors can be extracted by repeating this process for different sequences, initial states and measurements, as we will see below.

Assume that we aim to implement a set of unitary quantum gates. In reality, the hardware will realise perturbed gates, which we still assume to be unitary.

Consider concretely a situation where only gates in the set $\{\mathrm{CNOT}, \mathrm{X}_\theta^{(1)}, \mathrm{Y}_\theta^{(1)}, \mathrm{X}_\theta^{(2)}, \mathrm{Y}_\theta^{(2)}\}$ can be applied, namely a global CNOT and arbitrary single-qubit rotations around X- and Y-axis. Here, the superscripts indicate on which qubit the gate is applied, and the gates are defined as

$$\mathrm{CNOT} := |0\rangle\langle 0| \otimes \mathbb{I} + |1\rangle\langle 1| \otimes \sigma_1, \;\; X_\theta := e^{-i\frac{\theta}{2}\sigma_1}, \;\; Y_\theta := e^{-i\frac{\theta}{2}\sigma_2},$$

where σ_1, σ_2, σ_3 are the Pauli matrices. We assume that all single-qubit gates are already calibrated, and thus here, we want to use GSC to tune a perturbed CNOT gate, which we denote as $\tilde{\mathrm{CNOT}}$. The deviation from the optimal gate is measured by the *coherent error operator* associated with the gate. In the particular case of the CNOT gate we define

$$E := \mathrm{CNOT}^{-1}\tilde{\mathrm{CNOT}}. \tag{4.1}$$

In order to analyse the perturbed gate, we expand the error operator in the Pauli basis

$$E(\vec{p}) = \mathbb{I} - i\sum_{k=1}^{15} p_k \tau_k,$$

for suitable coefficients $\vec{p}$, which we call *error parameters*, and for $\tau_k = \tau_{ij} = \sigma_i \otimes \sigma_j$ with $\sigma_0 = \mathbb{I}$. The choice of the prefactor of the sum will ensure later that the unitarity of E to first order implies that p_k are real.

The ultimate goal of GSC is to obtain the error parameters, $\vec{p}$. To estimate the error parameters, GSC considers a number of experimental settings, which we label with the letter s. These settings can vary in the initial state, the gate sequence, and the measurement. We will always take $\rho = |00\rangle\langle 00|$ as initial state and perform a measurement $M_s \in \{\sigma_0 \otimes \sigma_3, \sigma_3 \otimes \sigma_0\}$.

Thus, for each setting one can experimentally estimate the quantity

$$R_s(\vec{p}) = \mathrm{Tr}\left[(G_{l_s,s}\cdots\tilde{\mathrm{CNOT}}(\vec{p})\cdots G_{1,s})|00\rangle\langle 00|(G_{1,s}^{\dagger}\cdots\tilde{\mathrm{CNOT}}(\vec{p})\cdots G_{l_s,s}^{\dagger})M_s\right], \tag{4.2}$$

which we will refer to as the *measurement response*. Here, l_s is the length of each sequence and $G_{j,s} \in \{\mathrm{X}_\theta^{(1)}, \mathrm{Y}_\theta^{(1)}, \mathrm{X}_\theta^{(2)}, \mathrm{Y}_\theta^{(2)}\}$ are the single-qubit gates of sequence s. Note that Eq. (4.2) does not restrict the number of CNOT gates of each sequence.

Following the framework of Ref. [39], we now make the assumption that the error parameters are small, and thus assume that the vector of responses depends only linearly on $\vec{p}$. We write

$$\vec{R}(\vec{p}) = \vec{R}(\vec{0}) + L\vec{p}, \tag{4.3}$$

where we define the matrix elements of L as

$$L_{su} := \left.\frac{\partial R_s(\vec{p})}{\partial p_u}\right|_{\vec{p}=\vec{0}}. \tag{4.4}$$

These matrix elements, L_{su}, as well as the vector $\vec{R}(\vec{0})$ can be computed analytically. Therefore, given the perturbed responses, $\vec{R}(\vec{p})$, we obtain the gate errors parameters by solving the inverse problem

$$\vec{p} = L^{-1}\left[\vec{R}(\vec{p}) - \vec{R}(\vec{0})\right]. \tag{4.5}$$

To ensure that the matrix L is non-singular, the number of responses must be equal to or greater than the number of error parameters. When this is not the case, additional responses can be added by considering more sequences, initial states or measurements. Moreover, the condition number of L must not be too large so that computing L^{-1} is numerically stable.

Having introduced the basic setup, we are now able to explain more clearly the motivation of this research. Table 4.1 summarises the combination of sequences and measurements used in Ref. [39] to calibrate a perturbed CNOT employing GSC. In the third column of Tab. 4.1, we see that the settings chosen consider only responses distributed around zero. Put differently, $R_s(\vec{0}) = 0$ for all $s = 1, \ldots, 15$. It turns out that, if one looks at statistics, this is also the point of maximal uncertainty since the variance of the responses is maximal for $R_s(\vec{0}) = 0$ (see Fig. 4.1). In fact, it is not obvious what the optimal point is, i.e., which settings of GSC minimise the statistical error and, at the same time, ensure stability of the numerical inverse of L and implementability of the protocol. Our research looks into this trade-off between reducing the statistical error, but still having a well-conditioned matrix L. Although we only consider the calibration of a two-qubit gate, the statistical analysis performed in the following sections can be generalised to higher dimensions straightforward.

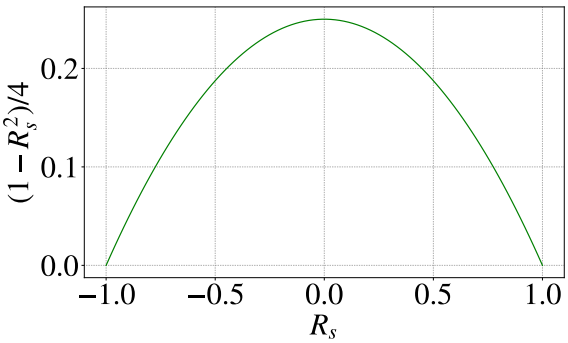

Figure 4.1: Variance of a estimated response, R_s^*, times the number of repetitions, N, as a function of the expectation value, R_s (see Eq. (4.6)).

4.2 The statistics of GSC

Quantum mechanics is unable to predict with certainty future events, such as measurement outcomes. Therefore, as we do in this section, it is essential to consider the statistics of the problem one is investigating to minimise statistical errors. Here, we study the statistics of GSC by determining the probability distribution according to which the measurement responses are distributed, as well as the error parameters. Subsequently, we define a quality measure that will allow us to compare the statistical error between different versions of GSC.

Before starting the discussion about GSC statistics, let us establish that all estimated quantities will be denoted by a superscript $*$. Assuming independent measurements, the outcome of a measurement with only two possible outcomes is described by a binomial distribution, $B(N, q)$, where N is the number of repetitions and q the probability of obtaining the outcome. In the scenario presented in Section 4.1, fifteen measurements are performed, one per setting, and each one is repeated N times. Therefore, the overall outcome is described by a multivariate binomial distribution. The CLT, reviewed in Sec. 3.1.1, states that binomial distribution can be approximated by a Gaussian distribution such that $\mathcal{N}(Nq, Nq(1-q))$ in the limit of sufficiently large N. Our interest is, in particular, focused on spin qubits, which are considered in Ref. [39] and where a high number of repetitions is easy to obtain. Therefore, we can assume that the overall GSC outcome can be approximated by a multivariate Gaussian distribution. We assume specifically that the estimated vector of responses is distributed as $\vec{R}^*(\vec{p}) \sim \mathcal{N}(\vec{R}(\vec{p}), \Sigma)$, where

$$\Sigma_{su} = \frac{1 - R_s^2(\vec{p})}{4N}\delta_{su}, \tag{4.6}$$

with $R_s(\vec{p})$ defined in Eq. (4.2). Note that the covariance matrix Σ is diagonal, i.e., settings are independent of each other.

s	1st gate	2nd gate	3rd gate	4th gate	M_s	$R_s(\vec{p})/2$
1	CNOT	$\mathrm{X}^{(1)}_{\pi/2}$			τ_{12}	$0 - p_5 + p_{10}$
2	$\mathrm{X}^{(1)}_{\pi/2}$	CNOT			τ_{12}	$0 - p_4 - p_7$
3	CNOT	$\mathrm{Y}^{(1)}_{\pi/2}$			τ_{12}	$0 - p_6 - p_9$
4	$\mathrm{Y}^{(1)}_{\pi/2}$	CNOT			τ_{12}	$0 - p_8 - p_{11}$
5	CNOT	$\mathrm{X}^{(2)}_{\pi/2}$			τ_3	$0 - p_1 - p_{13}$
6	CNOT	$\mathrm{Y}^{(2)}_{\pi/2}$			τ_3	$0 - p_2 - p_{14}$
7	$\mathrm{X}^{(1)}_{\pi/2}$	CNOT	$\mathrm{X}^{(1)}_{\pi/2}$		τ_{12}	$0 - p_2 + p_{10}$
8	$\mathrm{X}^{(1)}_{\pi/2}$	CNOT	$\mathrm{Y}^{(1)}_{\pi/2}$		τ_{12}	$0 - p_6 - p_{13}$
9	$\mathrm{Y}^{(1)}_{\pi/2}$	CNOT	$\mathrm{X}^{(1)}_{\pi/2}$		τ_{12}	$0 + p_{10} + p_{13}$
10	$\mathrm{X}^{(1)}_{\pi/2}$	$\mathrm{X}^{(2)}_{\pi/2}$	CNOT		τ_3	$0 - p_7 - p_{13}$
11	$\mathrm{Y}^{(1)}_{\pi/2}$	CNOT	$\mathrm{Y}^{(1)}_{\pi/2}$		τ_{12}	$0 - p_2 - p_6$
12	$\mathrm{Y}^{(1)}_{\pi/2}$	$\mathrm{Y}^{(2)}_{\pi/2}$	CNOT		τ_3	$0 - p_{11} - p_{14}$
13	$\mathrm{Y}^{(2)}_{\pi/2}$	CNOT	$\mathrm{X}^{(2)}_{\pi/2}$		τ_3	$0 + p_3 + p_{15}$
14	$\mathrm{X}^{(1)}_{\pi/2}$	CNOT	CNOT	$\mathrm{Y}^{(1)}_{\pi/2}$	τ_{12}	$0 - p_3 - 2p_{12} - p_{15}$
15	$\mathrm{X}^{(1)}_{\pi/2}$	$\mathrm{Y}^{(2)}_{\pi/2}$	CNOT	$\mathrm{X}^{(2)}_{\pi/2}$	τ_3	$0 - p_6 + p_{15}$

Table 4.1: Settings used in Ref. [39] to calibrate a $\tilde{\mathrm{CNOT}}$ gate (Eq. (4.1)) via GSC. Each row corresponds to one setting, where gates are applied from left to right and followed by a measurement (either $\tau_3 = \sigma_0 \otimes \sigma_3$ or $\tau_{12} = \sigma_3 \otimes \sigma_0$). The last column contains the measurement responses, which depend on the error parameters, $\vec{p}$ (see Eqns. (4.2) and (4.3)).

The estimated error parameters, $\vec{p}^*$, are computed with Eq. (4.5) using the estimated responses, $\vec{R}^*$, obtained from the lab. Therefore, $\vec{p}^*$ is a random vector distributed according to a multivariate Gaussian distribution with $\vec{p}^* \sim \mathcal{N}(\vec{p}, \Sigma_{\vec{p}^*})$, where

$$\Sigma_{\vec{p}^*} := L^{-1}\Sigma L^{-T}, \tag{4.7}$$

with $L^{-T} := (L^{-1})^T$. In App. 4.A, we give numerical evidences that support this theory.

In order to quantify the statistical error, we need to construct a measure of uncertainty. We take our quality measure to be the mean squared distance between $\vec{p}^*$ and $\vec{p}$, i.e.,

$$\langle D^2 \rangle := \langle ||\vec{p}^* - \vec{p}||^2 \rangle = \sum_{s=1}^{15} \langle (p_s^* - p_s)^2 \rangle = \sum_{s=1}^{15} \Sigma^{(ss)}_{\vec{p}^* - \vec{p}}\,, \tag{4.8}$$

$$= \mathrm{Tr}\, \Sigma_{\vec{p}^* - \vec{p}} = \mathrm{Tr}(L^{-1}\Sigma L^{-T}), \tag{4.9}$$

where $\Sigma_{\vec{p}^* - \vec{p}}$ is the covariance matrix of the random vector $\vec{p}^* - \vec{p}$ with matrix elements $\Sigma^{(su)}_{\vec{p}^* - \vec{p}}$. Note that $\langle \vec{p}^* - \vec{p} \rangle = \vec{0}$ since $\langle \vec{p}^* \rangle = \vec{p}$, which we have used in the second equality. Note further that $\Sigma_{\vec{p}^* - \vec{p}} = \Sigma_{\vec{p}^*}$ is given in Eq. (4.7). We extend the definition of $\langle D^2 \rangle$ to singular L by defining it to be ∞ in this case.

Now that we have characterised the statistics of GSC and defined a quality measure, we are able to minimise the statistical error of GSC. In the next section, we will look for a set of sequences, initial states and measurements which achieves a small mean squared distance under the restrictions that, first, L is a well-conditioned matrix and, second, the settings of GSC are physically implementable.

4.3 Optimising GSC

In this section, we employ the statistical characterisation we have developed in Sec. 4.2 to optimise the calibration protocol GSC. To do so, we introduce some parameters in the settings of GSC and minimise the statistical error over these parameters. Aiming for a physical implementation of GSC, we further modify the optimised settings to have a small number of different gates. Before all this, however, we start analysing the version of GSC proposed in Ref. [39] with the quality measure defined in Sec. 4.2.

In Ref. [39], GSC is introduced and applied to calibrate a perturbed two-qubit CNOT gate, as we have summarised in Sec. 4.1. Evaluating the statistical error of this version of the protocol in terms of the mean squared distance defined in Eq. (4.8), we obtain that $\langle D^2 \rangle \approx 1.8/N$.

As we have already mentioned in Sec. 4.2, we can assume that each estimated response, R_s^*, is distributed according to a Gaussian distribution such that $\mathcal{N}(R_s(\vec{p}), \Sigma_{ss})$ with $R_s(\vec{p})$ and Σ_{ss} defined in Eqns. (4.2) and (4.6), respectively. In Sec. 4.1, we have pointed out that, for the settings chosen in Ref. [39], each estimated response is distributed around zero when $\vec{p} = \vec{0}$ (see the last column of Tab. 4.1). The calibration of the CNOT is, therefore, performed at the point of maximal uncertainty, i.e., where the variance of each response reaches its maximum, $\Sigma_{ss} = 1/(4N)$, as we can see in Fig. 4.1. Here we have restricted the attention to the diagonal elements of Σ because all settings are independent of each other.

We propose to slightly modify GSC in order to benefit from working at a point with smaller statistical error. To this end, we allow a different angle for each rotation of each GSC sequence so that the calibration of a $\tilde{\text{CNOT}}$ is performed using the sequences in Tab. 4.2. Our idea is to numerically minimise the mean squared distance of these settings over the angles $\theta_1, \ldots, \theta_{25}$. Motivation for this optimisation strategy can be found in App. 4.C.

We use a local derivative-free optimiser specified as NLOPT_LN_BOBYQA in the NLopt library [68], which, according to the documentation, is derived from the BOBYQA subroutine introduced in Ref. [69]. This algorithm optimises the objective function by iteratively constructing its quadratic approximation. We set boundary constraints such that $\theta_i \in [0, 2\pi]$ for all $i = 1, \ldots, 25$. A stopping tolerance for the optimiser is set to 10^{-10} at the angles. Note that a local optimiser such as BOBYQA does not always converge to a global minimum. In order to gain confidence that our result is indeed a global minimum, we have repeated the optimisation 10^4 times with random starting points. In roughly one in 30 runs, the optimiser stopped at values within a factor of 10^{-5} of the smallest mean squared error observed. The code developed for this project is available in [70] and, in Appendix 4.D, we present essential parts of the code.

We obtain a minimum mean squared distance of $\langle D^2 \rangle \approx 0.84/N$ with the angles shown in Fig. 4.2. The numerical values of the angles are in Appendix 4.E. This result means that one can achieve a reduction of the statistical error of GSC by a factor of 0.47 with respect to the version of GSC proposed in Ref. [39].

The new version of GSC requires sixteen single-qubit rotations for a maximal sequence depth of four gates. Specifically, we need one rotation for each different angle and, for some angles, we need two rotations: one rotation around the X-axis and one rotation around the Y-axis. Note that, although all rotations $\mathrm{X}_{n\phi}$ and $\mathrm{Y}_{n\phi}$, where n is an integer, can be implemented by applying n times the rotation X_ϕ or Y_ϕ, respectively, this implies a cost in the sequence depth. Indeed, we can reduce the number of single-qubit rotations to twelve but with a cost of increasing the sequence depth to seven gates.

s	1st gate	2nd gate	3rd gate	4th gate	M_s
1	CNOT	$\mathrm{X}^{(1)}_{\theta_{15}}$			τ_{12}
2	$\mathrm{X}^{(1)}_{\theta_1}$	CNOT			τ_{12}
3	CNOT	$\mathrm{Y}^{(1)}_{\theta_{16}}$			τ_{12}
4	$\mathrm{Y}^{(1)}_{\theta_2}$	CNOT			τ_{12}
5	CNOT	$\mathrm{X}^{(2)}_{\theta_{17}}$			τ_3
6	CNOT	$\mathrm{Y}^{(2)}_{\theta_{18}}$			τ_3
7	$\mathrm{X}^{(1)}_{\theta_3}$	CNOT	$\mathrm{X}^{(1)}_{\theta_{19}}$		τ_{12}
8	$\mathrm{X}^{(1)}_{\theta_4}$	CNOT	$\mathrm{Y}^{(1)}_{\theta_{20}}$		τ_{12}
9	$\mathrm{Y}^{(1)}_{\theta_5}$	CNOT	$\mathrm{X}^{(1)}_{\theta_{21}}$		τ_{12}
10	$\mathrm{X}^{(1)}_{\theta_6}$	$\mathrm{X}^{(2)}_{\theta_7}$	CNOT		τ_3
11	$\mathrm{Y}^{(1)}_{\theta_8}$	CNOT	$\mathrm{Y}^{(1)}_{\theta_{22}}$		τ_{12}
12	$\mathrm{Y}^{(1)}_{\theta_9}$	$\mathrm{Y}^{(2)}_{\theta_{10}}$	CNOT		τ_3
13	$\mathrm{Y}^{(2)}_{\theta_{11}}$	CNOT	$\mathrm{X}^{(2)}_{\theta_{23}}$		τ_3
14	$\mathrm{X}^{(1)}_{\theta_{12}}$	CNOT	CNOT	$\mathrm{Y}^{(1)}_{\theta_{24}}$	τ_{12}
15	$\mathrm{X}^{(1)}_{\theta_{13}}$	$\mathrm{Y}^{(2)}_{\theta_{14}}$	CNOT	$\mathrm{X}^{(2)}_{\theta_{25}}$	τ_3

Table 4.2: Settings to optimise the calibration of a $\mathrm{C\tilde{N}OT}$ gate in Eq. (4.1) via GSC. A numerical optimisation over $\theta_1, \ldots, \theta_{25}$ allows to reduce the statistical error with respect to the GSC with settings in Tab. 4.1. For clarity, the responses of the measurements are in Appendix 4.B.

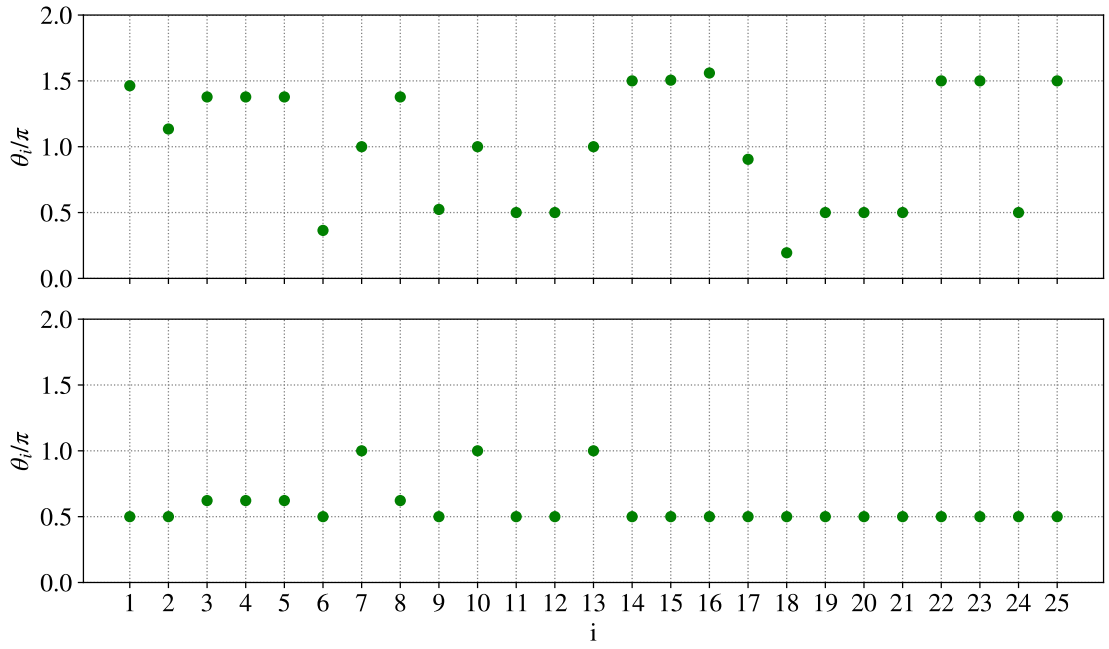

Figure 4.2: Above, angles that minimise the mean squared distance of the calibration of a $\widetilde{\text{CNOT}}$ using settings in Tab. 4.2 (Eq. (4.8)). Below, angles proposed here to optimise GSC. The angles below are the same angles as above after a folding transformation (i.e., mapping $\theta_i \longrightarrow 2\pi - \theta_i$ for all $\theta_i > \pi$) and setting $\theta_1 = \theta_2 = \theta_6 = \theta_9 = \theta_{15} = \theta_{16} = \theta_{17} = \theta_{18} = \pi/2$. Since the mean squared distance is invariant under folding transformation and independent of θ_1, θ_2, θ_6, θ_9, θ_{15}, θ_{16}, θ_{17}, θ_{18}, both angle combinations achieve the minimum mean squared distance, $\langle D^2 \rangle \approx 0.84/N$. The numerical values of the angles are in Appendix 4.E.

From an experimental point of view, tuning and calibrating sixteen different single-qubit rotations is undesirable. Hence, we would like to reduce the number of angles without increasing significantly the mean squared distance. We have observed numerically that the mean squared distance is invariant under the following transformations of the set of *optimal* angles (the transformations are not symmetries of the objective function at non-optimal points):

1. *degeneracy*: any change of the angles θ_1, θ_2, θ_6, θ_9, θ_{15}, θ_{16}, θ_{17}, and θ_{18} as long as L remains non-singular;

2. *global reflection*: $\theta_i \longrightarrow 2\pi - \theta_i$ for all $i = 1, \ldots, 25$;

3. *local reflection*: $\theta_i \longrightarrow 2\pi - \theta_i$ for one $i \in \{1, \ldots, 25\}$ as long as L remains non-singular;

4. *folding transformation*: $\theta_i \longrightarrow 2\pi - \theta_i$ for all $\theta_i > \pi$.

It would be tempting to set all the angles listed under 1. to zero, thereby eliminating the corresponding gates. However, it turns out that this choice does lead to a singular L and will therefore not be considered here. Still, a significant reduction of complexity can be achieved by making use of the above symmetries. The folding transformation allows us to reduce the

number of different rotations to thirteen for a maximal sequence depth of four gates without cost in the mean squared distance. At the price of increasing the sequence depth to seven gates, one can further reduce to eleven distinct rotations.

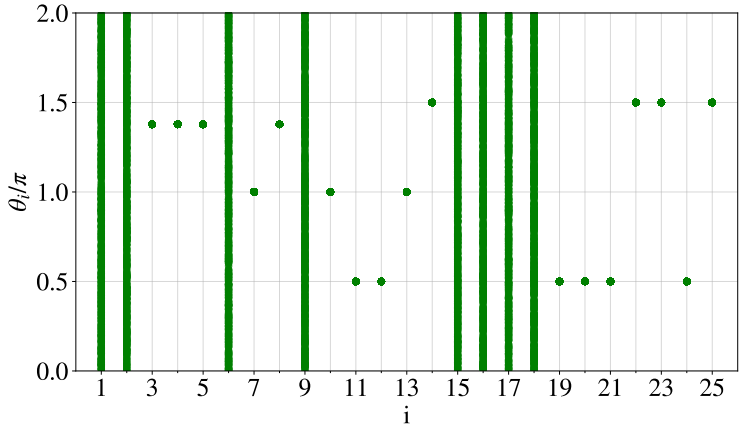

Figure 4.3: Combinations of angles that give a mean squared distance $\langle D^2 \rangle \approx 0.84/N$. The mean squared distance is independent of θ_1, θ_2, θ_6, θ_9, θ_{15}, θ_{16}, θ_{17}, θ_{18}, and thus we can set these angles at any value in $[0, 2\pi]$ without any cost in the statistical error.

To reduce even more the number of necessary gates, we use the fact that the minimum mean squared distance is degenerate. In Fig. 4.3, we can see that the minimum mean squared distance is achieved regardless of the value of the angles θ_1, θ_2, θ_6, θ_9, θ_{15}, θ_{16}, θ_{17} and θ_{18}. As we can unfortunately not set these angles simply to zero, we set them to $\pi/2$, which is a single-qubit gate already required to implement GSC (see Fig. 4.2). The mean squared distance remains at $\langle D^2 \rangle \approx 0.84/N$, and now GSC needs only four rotations and a maximal sequence depth of five gates.

Ultimately, we propose a GSC protocol that calibrates a $\widetilde{\text{CNOT}}$ gate with a statistical error 0.47 times smaller than in Ref. [39]. The maximal sequence depth is five and the set of allowed gates is $\{\text{CNOT}, \text{X}^{(1)}_{\pi/2}, \text{Y}^{(1)}_{\pi/2}, \text{X}^{(2)}_{\pi/2}, \text{Y}^{(2)}_{\pi/2}, \text{X}^{(1)}_{\theta}, \text{Y}^{(1)}_{\theta}\}$, where $\theta = 0.62208\pi$, as we see in Tab. 4.3.

4.3.1 GSC with imperfect measurements

In all previous sections, the measurements performed in GSC are assumed to be perfect. In other words, we have assumed that the measurement outcome obtained by the measurement device always corresponds to the state after the measurement. However, in the laboratory, devices are imperfect and, therefore, there is a non-zero error probability, i.e., a probability of obtaining a measurement outcome that differs from the true outcome corresponding to the post-measurement state. With the intention of building a model as realistic as possible, we introduce imperfect measurements in GSC along this section.

s	1st gate	2nd gate	3rd gate	4th gate	5th gate	M_s	$R_s(\vec{p})/2$
1	CNOT	$\mathrm{X}^{(1)}_{\pi/2}$				τ_{12}	$0 - p_5 + p_{10}$
2	$\mathrm{X}^{(1)}_{\pi/2}$	CNOT				τ_{12}	$0 - p_4 - p_7$
3	CNOT	$\mathrm{Y}^{(1)}_{\pi/2}$				τ_{12}	$0 - p_6 - p_9$
4	$\mathrm{Y}^{(1)}_{\pi/2}$	CNOT				τ_{12}	$0 - p_8 - p_{11}$
5	CNOT	$\mathrm{X}^{(2)}_{\pi/2}$				τ_3	$0 - p_1 - p_{13}$
6	CNOT	$\mathrm{Y}^{(2)}_{\pi/2}$				τ_3	$0 - p_2 - p_{14}$
7	$\mathrm{X}^{(1)}_{\theta}$	CNOT	$\mathrm{X}^{(1)}_{\pi/2}$			τ_{12}	$0 - \sin\theta p_2 - \cos\theta p_5 + p_{10}$
8	$\mathrm{X}^{(1)}_{\theta}$	CNOT	$\mathrm{Y}^{(1)}_{\pi/2}$			τ_{12}	$0 - p_6 - \cos\theta p_9 - \sin\theta p_{13}$
9	$\mathrm{Y}^{(1)}_{\theta}$	CNOT	$\mathrm{X}^{(1)}_{\pi/2}$			τ_{12}	$0 - \cos\theta p_5 + p_{10} + \sin\theta p_{13}$
10	$\mathrm{X}^{(1)}_{\pi/2}$	$\mathrm{X}^{(2)}_{\pi/2}$	$\mathrm{X}^{(2)}_{\pi/2}$	CNOT		τ_3	$0 + p_4 - p_7$
11	$\mathrm{Y}^{(1)}_{\theta}$	CNOT	$\mathrm{Y}^{(1)}_{\pi/2}$			τ_{12}	$0 - \sin\theta p_2 - p_6 - \cos\theta p_9$
12	$\mathrm{Y}^{(1)}_{\pi/2}$	$\mathrm{Y}^{(2)}_{\pi/2}$	$\mathrm{Y}^{(2)}_{\pi/2}$	CNOT		τ_3	$0 + p_8 - p_{11}$
13	$\mathrm{Y}^{(2)}_{\pi/2}$	CNOT	$\mathrm{X}^{(2)}_{\pi/2}$			τ_3	$0 + p_3 + p_{15}$
14	$\mathrm{X}^{(1)}_{\pi/2}$	CNOT	CNOT	$\mathrm{Y}^{(1)}_{\pi/2}$		τ_{12}	$0 - p_3 - 2p_{12} - p_{15}$
15	$\mathrm{X}^{(1)}_{\pi/2}$	$\mathrm{X}^{(1)}_{\pi/2}$	$\mathrm{Y}^{(2)}_{\pi/2}$	CNOT	$\mathrm{X}^{(2)}_{\pi/2}$	τ_3	$0 - p_3 + p_{15}$

Table 4.3: Settings proposed to reduce the statistical error in the calibration of a $\tilde{\mathrm{CNOT}}$ using GSC. The set of allowed gates is $\{\mathrm{CNOT}, \mathrm{X}^{(1)}_{\pi/2}, \mathrm{Y}^{(1)}_{\pi/2}, \mathrm{X}^{(2)}_{\pi/2}, \mathrm{Y}^{(2)}_{\pi/2}, \mathrm{X}^{(1)}_{\theta}, \mathrm{Y}^{(1)}_{\theta}\}$ with $\theta = 0.62208\pi$.

Consider the scenario presented in Sec. 4.1: calibrating a perturbed gate, $\tilde{\text{CNOT}}$, (see Eq. (4.1)) using GSC. All measurements performed in GSC are Pauli observables, and thus they have only two outcomes, the positive and the negative outcome. We now consider an imperfect measurement device and allow a different error probability for each outcome. In other words, the measurement device gives the correct outcome $i \in \{\pm\}$ with a probability F_i, and an incorrect outcome with probability $1 - F_i$.

The probability to read a positive outcome on the measurement device after measuring M_s is then

$$\begin{aligned} Q_s(+) :=& F_+ q_s + (1 - F_-)(1 - q_s), \\ =& \frac{1}{2}\left[1 + F_+ - F_- + R_s\left(F_+ + F_- - 1\right)\right], \end{aligned}$$

where q_s is the probability of the positive outcome, i.e., $q_s = (1 + R_s)/2$, and R_s is defined in Eq. (4.2). Recall that R_s depends on the error parameters, and so do q_s and $Q_s(+)$.

The probability that the measurement device gives a negative outcome after performing the measurement M_s is

$$\begin{aligned} Q_s(-) =& F_-(1 - q_s) + (1 - F_+)q_s, \\ =& \frac{1}{2}\left[1 + F_- - F_+ - R_s\left(F_+ + F_- - 1\right)\right]. \end{aligned}$$

It is easy to check that $Q_s(+) + Q_s(-) = 1$.

The *imperfect measurement responses* are hence given by

$$\begin{aligned} \tilde{R}_s(\vec{p}) &= Q(+) - Q(-), \\ &= F_+ - F_- + R_s(F_+ + F_- - 1). \end{aligned}$$

Then, the matrix elements of L can be written as

$$\tilde{L}_{ru} = \left.\frac{\partial \tilde{R}_r(\vec{p})}{\partial p_u}\right|_{\vec{p}=\vec{0}}, \tag{4.10}$$

$$= (F_+ + F_- - 1)L_{ru}. \tag{4.11}$$

For imperfect measurements we also use the mean squared distance as measure of uncertainty to compare different versions of GSC. The mean squared distance considering imperfect measurements becomes

$$\langle \tilde{D}^2 \rangle = \text{Tr}(\tilde{L}^{-1}\tilde{\Sigma}\tilde{L}^{-T}), \tag{4.12}$$

where the matrix elements of the covariance matrix of the perturbed measurement responses, $\tilde{\Sigma}$, are $\tilde{\Sigma}_{su} = \frac{1}{4N}(1 - \tilde{R}_s^2)\delta_{su}$.

Let $F_+ = 0.99$ and $F_- = 0.98$ and consider the GSC presented in Ref. [39], which uses the sequences in Tab. 4.1. The statistical error measured by the mean squared distance in Eq. (4.12) is $\langle \tilde{D}^2 \rangle \approx 2.0/N$.

Allow now a different angle for each GSC rotation, i.e., consider the sequences in Tab. 4.2. With the optimisation procedure described for the case of perfect measurement, we minimise the mean squared distance in Eq. (4.12) over the angles $\theta_1, \ldots, \theta_{25}$. The angles in Fig. 4.4 achieve a minimal mean squared distance at $\langle \tilde{D}^2 \rangle \approx 0.89/N$. This means a statistical error 0.45 times smaller than in Ref. [39], but requires seventeen different rotations with a maximal sequence depth of four gates. Assuming a cost of a sequence depth of seven gates, we can decrease the number of rotations to thirteen.

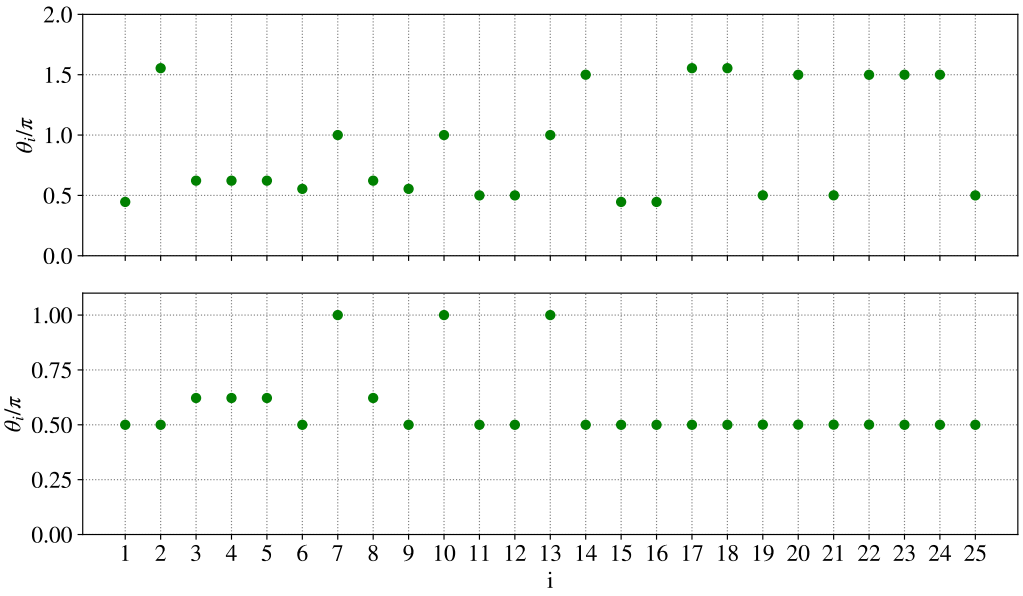

Figure 4.4: Above, angles that minimise the mean squared distance in Eq. (4.12), which considers imperfect measurements in the calibration of a $\tilde{\text{CNOT}}$ using sequences in Tab. 4.2. Below, angles proposed here to optimise GSC considering imperfect measurement. The angles below are the same angles as above after a folding transformation (i.e., mapping $\theta_i \longrightarrow 2\pi - \theta_i$ for all $\theta_i > \pi$) and setting $\theta_1 = \theta_2 = \theta_6 = \theta_9 = \theta_{15} = \theta_{16} = \theta_{17} = \theta_{18} = \pi/2$.

Analogous to the case with perfect measurements, the number of rotations can be reduced by considering symmetries of the optimal mean squared distance. We have numerically shown that the minimal $\langle \tilde{D}^2 \rangle$ is invariant under folding transformation as well as global and local reflection of the *optimal* angles. After considering the folding transformation, the number of rotations reduces to twelve without any change in the mean squared distance and a maximal sequence depth of four gates.

If twelve different single-qubit rotations are undesirable to perform in the lab, we can set the angles $\theta_1 = \theta_2 = \theta_6 = \theta_9 = \theta_{15} = \theta_{16} = \theta_{17} = \theta_{18} = \pi/2$. In contrast to the case of per-

fect measurements, the mean squared distance for imperfect measurement is not degenerated. Therefore, setting these angles implies an increase of the statistical error to $\langle \tilde{D}^2 \rangle \approx 0.90/N$. This means, however, still a reduction of the statistical error by a factor of 0.45 with respect to the statistical error in Ref. [39]. Note that the final settings suggested for GSC are the same in both cases, considering perfect and imperfect measurements.

In summary, we propose to calibrate a perturbed CNOT using GSC with the sequences in Tab. 4.3 and $\theta = 0.62208\pi$. This version of GSC requires a maximal sequence depth of five gates and a set of allowed gates consisting of $\{\mathrm{CNOT}, \mathrm{X}^{(1)}_{\pi/2}, \mathrm{Y}^{(1)}_{\pi/2}, \mathrm{X}^{(2)}_{\pi/2}, \mathrm{Y}^{(2)}_{\pi/2}, \mathrm{X}^{(1)}_{\theta}, \mathrm{Y}^{(1)}_{\theta}\}$, which contains two more single-qubit gates than the set proposed in Ref. [39]. Nevertheless, it reduces the statistical error by a factor of 0.47 for perfect measurements and a factor of 0.45 for imperfect measurements, with $F_+ = 0.99$ and $F_- = 0.98$. All results are compiled in Tab. 4.4.

	$[F_+, F_-]$	$\langle D^2 \rangle \cdot N$	# rotations	Maximal sequence depth
Angles of Ref. [39]	$[1, 1]$	1.8	2	4
Optimal angles	$[1, 1]$	0.84	17	4
Folded angles	$[1, 1]$	0.84	12	4
Modified angles	$[1, 1]$	0.84	4	5
Angles of Ref. [39]	$[0.99, 0.98]$	2.0	2	4
Optimal angles	$[0.99, 0.98]$	0.89	17	4
Folded angles	$[0.99, 0.98]$	0.89	12	4
Modified angles	$[0.99, 0.98]$	0.90	4	5

Table 4.4: Summary of numerical results, where the statistical error is measured by the mean squared distance, $\langle D^2 \rangle$. The last two columns show the number of single-qubit rotations that must be available and the maximal sequence depth for each version of GSC.

4.4 Conclusions and outlook

We have seen that optimising the design of an experiment is crucial for minimising statistical errors. In particular, we have used DOE to propose a new version of GSC that reduces the statistical error by a factor of 0.47 for perfect measurements and by a factor of 0.45 for imperfect measurements. To achieve this, one initial state, two Pauli measurements and six single-qubit rotations must be available.

Several questions remain open. Although we have reduced the statistical error, a physical explanation of the optimal sequences is still missing. We also do not know why the mean squared distance is degenerate for perfect measurements and why the degeneracy breaks down for imperfect measurements (even when $F_+ = F_- \neq 1$).

Our optimisation has been based on parmeterising the GSC sequences, but different initial states and measurements could also be considered. Furthermore, we have used fifteen settings to solve fifteen error parameters. Considering additional settings, however, and making a statistical treatment of the redundant information could further reduce the statistical error.

Finally, it would also be interesting to put our results into practice, and thus experimentally calibrate a $\tilde{\text{CNOT}}$ with the version of GSC proposed in this chapter.

Appendix

4.A Histograms of the error parameters

In Sec. 4.2, we have statistically analysed the calibration protocol GSC. Particularly assuming that the measurement responses follow a Gaussian distribution, we have determined the probability distribution of the error parameters. Here, we present some histograms of simulated data that support our statistical characterisation of GSC.

Making use of the CLT, we have determined in Sec. 4.2 that the vector of estimated responses, $\vec{R}^*(\vec{p})$, follows a multivariate Gaussian distribution such that $\vec{R}^*(\vec{p}) \sim \mathcal{N}(\vec{R}(\vec{p}), \Sigma)$, where the matrix elements of the Σ are given in Eq. (4.6). Consequently, the vector of estimated error parameters, $\vec{p}^*$, is also distributed according to a multivariate Gaussian distribution with $\vec{p}^* \sim \mathcal{N}(\vec{p}, \Sigma_{\vec{p}^*})$, where $\Sigma_{\vec{p}^*}$ is defined in Eq. (4.7). Recall that $\vec{p}^*$ can be computed with the affine transformation in Eq. (4.5) using the vector of estimated responses, $\vec{R}(\vec{p})^*$.

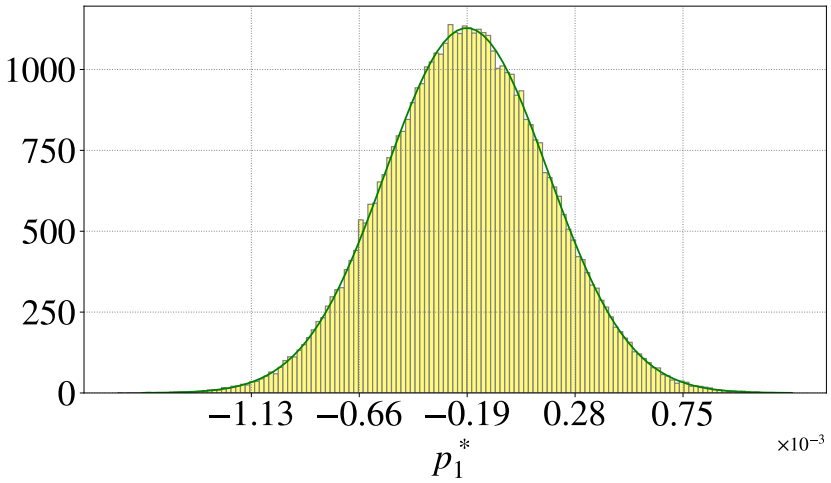

Figure 4.A.1: Histogram of the estimated error parameter p_1^* and, in green, Gaussian distribution with parameters $\mathcal{N}(p_1, \Sigma_{\vec{p}^*}^{(11)})$, where $\Sigma_{\vec{p}^*}^{(11)}$ is the first diagonal element of $\Sigma_{\vec{p}^*}$ defined in Eq. (4.7).

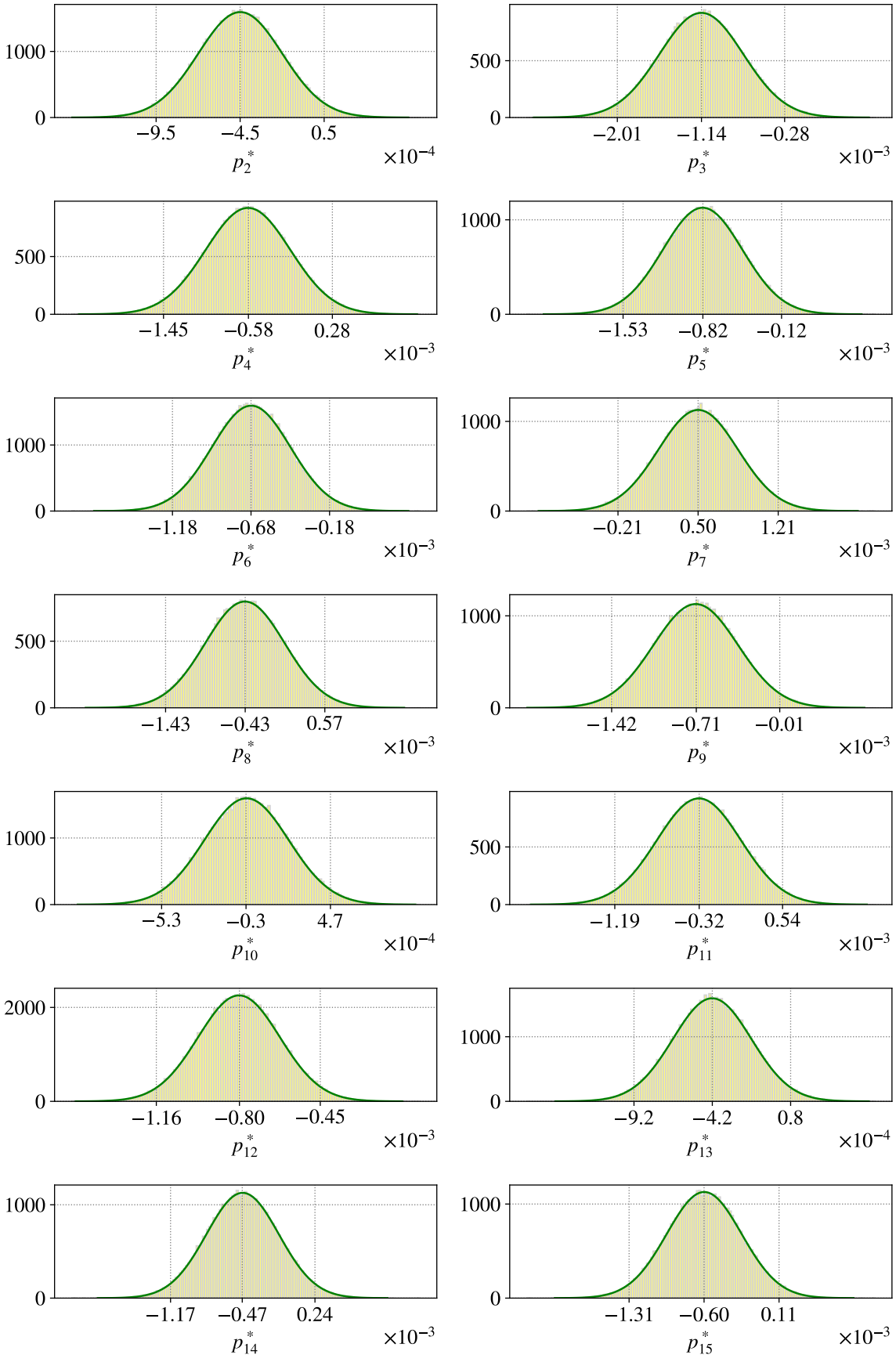

Figure 4.A.2: Histograms of the error parameters $p_2^*, \ldots, p_{15}^*$. In green, Gaussian distributions with parameters $\mathcal{N}(p_s, \Sigma_{\vec{p}^*}^{(ss)})$, where $\Sigma_{\vec{p}^*}^{(ss)}$ are the diagonal elements of $\Sigma_{\vec{p}^*}$ defined in Eq. (4.7).

To confirm the mean vector and the covariance matrix of the multivariate Gaussian distribution of $\vec{p}^*$ numerically, we simulate the calibration of a perturbed CNOT gate using the GSC introduced in Ref. [39]. Assuming the calibration with GSC is repeated $N = 10^6$ times in the lab, we perform the simulation 10^5 times. We compute the vector of estimated error parameters in each simulation and save it. With this data, we build a histogram for each estimated error parameter, p_s^* for $s = 1, \ldots, 15$. In Fig. 4.A.1, we show that the histogram of the error parameter p_1^* is compatible with the theoretically predicted Gaussian distribution $\mathcal{N}(p_1, \Sigma_{\vec{p}^*}^{(11)})$, where $\Sigma_{\vec{p}^*}^{(su)}$ are the matrix elements of $\Sigma_{\vec{p}^*}$. Analogous histograms of the estimated error parameters $p_2^*, \ldots, p_{15}^*$ are plotted apart for clarity in Fig. 4.A.2.

4.B Responses of Table 4.2

In Sec. 4.3, we have considered GSC with the settings summarised in Tab. 4.2. We present here the measurement responses corresponding to this protocol.

Using Eqns. (4.2) and (4.3), we obtain that the responses of the settings in Tab. 4.2 are given by

$$
\begin{aligned}
R_1(\vec{p}) &= \cos\theta_{15} - 2\cos\theta_{15}p_5 + 2\cos\theta_{15}p_{10},\\
R_2(\vec{p}) &= \cos\theta_1 - 2\cos\theta_1 p_4 - 2\cos\theta_1 p_7,\\
R_3(\vec{p}) &= \cos\theta_{16} - 2\cos\theta_{16}p_6 - 2\cos\theta_{16}p_9,\\
R_4(\vec{p}) &= \cos\theta_2 - 2\cos\theta_2 p_8 - 2\cos\theta_2 p_{11},\\
R_5(\vec{p}) &= \cos\theta_{17} - 2\cos\theta_{17}p_1 - 2\cos\theta_{17}p_{13},\\
R_6(\vec{p}) &= \cos\theta_{18} - 2\cos\theta_{18}p_2 - 2\cos\theta_{18}p_{14},\\
R_7(\vec{p}) &= \cos\theta_{19}\cos\theta_3 - 2\cos\theta_{19}\cos\theta_3 p_2 - 2\cos\theta_{19}\cos\theta_3 p_4\\
&\quad - 2\cos\theta_3\cos\theta_{19}p_5 - 2\cos\theta_{19}\cos\theta_3 p_7 + 2\cos\theta_{19}p_{10},\\
R_8(\vec{p}) &= \cos\theta_{20}\cos\theta_4 - 2\cos\theta_{20}\cos\theta_4 p_4 - 2\cos\theta_{20}p_6\\
&\quad - 2\cos\theta_{20}\cos\theta_4 p_7 - 2\cos\theta_4\cos\theta_{20}p_9 - 2\cos\theta_{20}\cos\theta_4 p_{13},\\
R_9(\vec{p}) &= \cos\theta_{21}\cos\theta_5 - 2\cos\theta_5\cos\theta_{21}p_5 - 2\cos\theta_{21}\cos\theta_5 p_8\\
&\quad + 2\cos\theta_{21}p_{10} - 2\cos\theta_{21}\cos\theta_5 p_{11} + 2\cos\theta_{21}\cos\theta_5 p_{13},\\
R_{10}(\vec{p}) &= \cos\theta_6\cos\theta_7 - 2\cos\theta_6 p_7 - 2\cos\theta_7\cos\theta_6 p_4\\
&\quad - 2\sin\theta_7 p_{13} - 2p_1\cos\theta_6\sin\theta_7,\\
R_{11}(\vec{p}) &= \cos\theta_{22}\cos\theta_8 - 2\cos\theta_{22}p_6 - 2\cos\theta_8\cos\theta_{22}p_9\\
&\quad - 2\cos\theta_{22}\cos\theta_8 p_{11} - 2\cos\theta_{22}\cos\theta_8 p_8 - 2\cos\theta_{22}\cos\theta_8 p_2,\\
R_{12}(\vec{p}) &= \cos\theta_{10}\cos\theta_9 - 2\cos\theta_9\cos\theta_{10}p_2 - 2\cos\theta_{10}\cos\theta_9 p_8\\
&\quad - 2\cos\theta_9 p_{11} - 2\cos\theta_{10}p_{14},
\end{aligned}
$$

$$
\begin{aligned}
R_{13}(\vec{p}) = &\cos\theta_{11}\cos\theta_{23} - 2\cos\theta_{11}\cos\theta_{23}p_1 - 2\cos\theta_{23}\cos\theta_{11}p_2 \\
&+ 2\cos\theta_{11}\cos\theta_{23}p_3 - 2\cos\theta_{11}\cos\theta_{23}p_{13} \\
&- 2\cos\theta_{23}\cos\theta_{11}p_{14} + 2\cos\theta_{11}\cos\theta_{23}p_{15}, \\
R_{14}(\vec{p}) = &\cos\theta_{12}\cos\theta_{24} - 2\cos\theta_{12}\cos\theta_{24}p_3 - 2\cos\theta_{24}\cos\theta_{12}p_4 \\
&- 2\cos\theta_{24}\cos\theta_{12}p_5 - 2\cos\theta_{12}\cos\theta_{24}p_6 \\
&- 2\cos\theta_{24}\cos\theta_{12}p_7 - 2\cos\theta_{12}\cos\theta_{24}p_8 \\
&- 2\cos\theta_{12}\cos\theta_{24}p_9 - 2\cos\theta_{12}\cos\theta_{24}p_{11} \\
&+ 2\cos\theta_{24}\cos\theta_{12}p_{10} - 4\cos\theta_{12}\cos\theta_{24}p_{12} \\
&- 2\cos\theta_{12}\cos\theta_{24}p_{15}, \\
R_{15}(\vec{p}) = &\cos\theta_{13}\cos\theta_{14}\cos\theta_{25} - 2\cos\theta_{25}\cos\theta_{13}p_7 - 2\cos\theta_{14}\cos\theta_{25}\cos\theta_{13}p_4 \\
&- 2\cos\theta_{25}\cos\theta_{14}p_{14} - 2\cos\theta_{13}\cos\theta_{25}\cos\theta_{14}p_2 \\
&- 2\cos\theta_{14}\cos\theta_{25}p_{13} - 2\cos\theta_{13}\cos\theta_{14}\cos\theta_{25}p_1 \\
&- 2\cos\theta_{13}\cos\theta_{25}p_6 + 2\cos\theta_{14}\cos\theta_{25}p_{15} \\
&+ 2\cos\theta_{13}\cos\theta_{14}\cos\theta_{25}p_3.
\end{aligned}
$$

4.C Statistical error as a function of the rotation angle

The optimisation of GSC performed in Sec. 4.3 has been carried out by allowing a different angle for each single-qubit rotation. Nevertheless, GSC permits not only changing the sequences of the settings but also the measurements and the initial states. Here, we present some motivation for our choice of optimisation strategy.

As we have mentioned in the main text, the goal of this project is to optimise GSC by minimising statistical errors. We intend, at the same time, to propose a new version of GSC that is physically feasible, and thus we aim to introduce small modifications on the original version of GSC. For this reason, we start considering the same set-up as in Ref. [39], i.e., the settings in Tab. 4.1. In this version of GSC all single-qubit gates are $\pi/2$-rotations, so a simple change on the protocol is considering a different rotation angle, which we denote as θ. Computing the mean squared distance of GSC, $\langle D^2 \rangle$ defined in Eq. (4.8), for different values of θ, we can plot the statistical error of GSC as a function of the rotation angle. In Fig. 4.C.1, we find that the choice made in Ref. [39], i.e., $\theta = \pi/2$, does not give the minimum mean squared distance, but the minimum $\langle D^2 \rangle$ is achieved for $\theta = 1.428\pi$ does.

In order to further reduce the statistical error, we have considered in Sec. 4.3 not only one rotation angle, but a different angle for each single-qubit rotation.

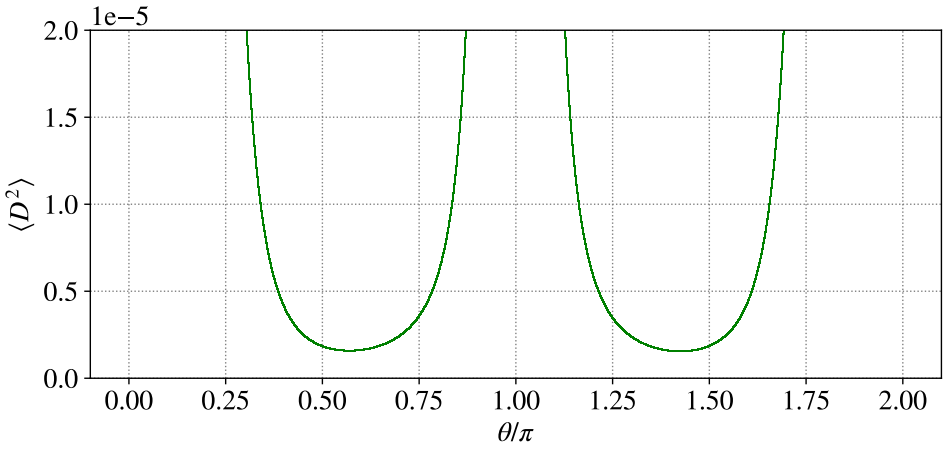

Figure 4.C.1: Mean squared distance, $\langle D^2 \rangle$ defined in Eq. (4.8), as a function of the single-qubit-rotation angle, θ.

4.D Optimisation code

Section 4.3 has been devoted to optimise GSC. Below we present the code that we developed and used for this optimisation.

```
import numpy as np
import nlopt as nlopt

import functions.basic_functions as bf
import functions.fake_data_functions as fd
import functions.optimisation_functions as opt

# OPTIMISATION OVER 25 ANGLES
M = 1*10**4 # Number of optimisations
F = [1, 1] # Measurement fidelities. If F=[1,1], perfect measurements.

list_result_code = [] # Initialise list for stopping criteria
list_opt_mean_distance2 = [] # Initialise list for mean squared distance
list_opt_vec_theta = [] # Initialise list for angles

for m in range(M):
    # When the optimiser runs into a RoundoffLimited error, the value of theta is skipped.
    try:
        # The initial point of the optimiser is chosen randomly.
        vec_theta0 = np.random.random(25)*2*np.pi
```

```
# Check if the initial value gives a non-singular L.
inv = bf.is_invertible(np.array(opt.L(vec_theta0,F)))
while inv == False:
    vec_theta0 = np.random.random(25) * 2 * np.pi
    inv = bf.is_invertible(opt.L(vec_theta0))

# (LOCAL) OPTIMISATION

# Choice of the optimiser and number of parameters to optimise
optL = nlopt.opt(nlopt.LN_BOBYQA, 25)

# Set max time for each optimisation
optL.set_maxtime(0.25*60*60)

# Set 0 as lower bound for the angles
optL.set_lower_bounds(np.zeros(25))

# Set 2*pi as upper bound for the angles
optL.set_upper_bounds([2*np.pi for i in range(25)])

# Choose the function called opt.mysuperfunc1 to minimise
optL.set_min_objective(opt.mysuperfunc1)

# Set tolerance for the angles
optL.set_xtol_rel(1e-10)

# Start optimisation with vec_theta0 as initial point and keep the optimal angles
opt_vec_theta = optL.optimize(vec_theta0)

# Keep optimised mean squared distance
opt_mean_distance2 = optL.last_optimum_value()

# Keep the stopping criteria
result_code_L = optL.last_optimize_result()

list_opt_vec_theta.append(opt_vec_theta)
list_opt_mean_distance2.append(opt_mean_distance2)
list_result_code.append(result_code_L)
```

```
    # Skip values of theta that produce a RoundoffLimited error
    except nlopt.RoundoffLimited:
        print("RoundoffLimited error at m=", m, ".")
        print("vec_theta0 =", vec_theta0)
        print("Value skipped.")
```

The code above optimises a function called `opt.mysuperfunc1`, which we have defined as

```
def mysuperfunc1(vec_theta, grad):
    N = 10**6 # Number of runs of the "experiment in the lab"
    F = [1, 1] # Measurement fidelities

    return mean_distance2(vec_theta, N, F)
```

where

```
def mean_distance2(vec_theta, N, F):
    # Constructing the matrix L
    matrix_L = L(vec_theta, F)

    # Constructing covariance matrix of responses
    cov_matrix = cov_matrixR(vec_theta, N, F)

    # If L is non-singular, the function computes the mean squared distance
    if bf.is_invertible(np.array(matrix_L))==True:
        D2 = np.matrix.trace(np.linalg.inv(matrix_L) @ cov_matrix @ np.matrix.transpose(np.
            ↪ linalg.inv(matrix_L)))
        return D2
    else: # If L is singular, the function returns infinity.
        return mth.inf
```

with the function `L(vec_theta,F)` computing the L matrix defined in Eq. (4.10).

4.E Optimal angles

In Sec. 4.3 we have optimised the calibration of a $\widetilde{\text{CNOT}}$ via GSC with sequences in Tab. 4.2 considering perfect and imperfect measurements. Here, the concrete values of $\theta_1, \ldots, \theta_{25}$ that achieve the minimal mean squared distance are presented for both cases.

With the optimisation process presented in Sec. 4.3, we have obtained a minimal squared distance in the case of perfect measurements (Eq. (4.8)) of $\langle D^2 \rangle \approx 0.84/N$ with the angles

$$
\begin{aligned}
\theta_1/\pi &= 1.3864, & \theta_2/\pi &= 0.3743,\\
\theta_3/\pi &= 1.3779, & \theta_4/\pi &= 1.3779,\\
\theta_5/\pi &= 1.3779, & \theta_6/\pi &= 1.5722,\\
\theta_7/\pi &= 1.0000, & \theta_8/\pi &= 1.3779,\\
\theta_9/\pi &= 0.4003, & \theta_{10}/\pi &= 1.0000,\\
\theta_{11}/\pi &= 0.5000, & \theta_{12}/\pi &= 1.5000,\\
\theta_{13}/\pi &= 1.0000, & \theta_{14}/\pi &= 0.5000,\\
\theta_{15}/\pi &= 1.0310, & \theta_{16}/\pi &= 0.2618,\\
\theta_{17}/\pi &= 0.3087, & \theta_{18}/\pi &= 0.8718,\\
\theta_{19}/\pi &= 0.5000, & \theta_{20}/\pi &= 0.5000,\\
\theta_{21}/\pi &= 0.5000, & \theta_{22}/\pi &= 1.5000,\\
\theta_{23}/\pi &= 0.5000, & \theta_{24}/\pi &= 0.5000,\\
\theta_{25}/\pi &= 1.5000.
\end{aligned}
$$

These angles are plotted in Fig. 4.2.

Using the same optimisation process, but the mean squared distance in Eq. (4.12), which considers imperfect measurements, we have obtained a minimum mean squared distance at $\langle \tilde{D}^2 \rangle \approx 0.89/N$ with the angles

$$
\begin{aligned}
\theta_1/\pi &= 0.4459, & \theta_2/\pi &= 0.4459,\\
\theta_3/\pi &= 1.3779, & \theta_4/\pi &= 1.3779,\\
\theta_5/\pi &= 0.6221, & \theta_6/\pi &= 0.5541,\\
\theta_7/\pi &= 1.0000, & \theta_8/\pi &= 0.6221,\\
\theta_9/\pi &= 0.5541, & \theta_{10}/\pi &= 1.0000,\\
\theta_{11}/\pi &= 1.5000, & \theta_{12}/\pi &= 0.5000,\\
\theta_{13}/\pi &= 1.0000, & \theta_{14}/\pi &= 1.5000,\\
\theta_{15}/\pi &= 1.5541, & \theta_{16}/\pi &= 0.4459,\\
\theta_{17}/\pi &= 1.5541, & \theta_{18}/\pi &= 0.4459,\\
\theta_{19}/\pi &= 1.4993, & \theta_{20}/\pi &= 0.5007,\\
\theta_{21}/\pi &= 0.5007, & \theta_{22}/\pi &= 1.4993,\\
\theta_{23}/\pi &= 1.5000, & \theta_{24}/\pi &= 0.5000,\\
\theta_{25}/\pi &= 1.5000.
\end{aligned}
$$

Figure 4.4 contains a plot of these angles.

Conclusions

This chapter summarises the results presented along the thesis and discusses future research as well as open questions. In accordance with the structure of the thesis, we divide the chapter into two sections, where each presents the conclusion of one part.

Classical restrictions of matrix product states

Summary

Physical interactions are local, and this locality is one of the most relevant factors that enforces which states are likely for low-energy physical systems. Matrix product states are an efficient representation of ground states of any gapped Hamiltonian. Not only do MPSs provide a complete framework for the most physically relevant Hamiltonians, but simulations based on MPSs are also highly precise and efficient. The efficiency and high precision of MPSs rely on the accurate description of correlations within the state, which are restricted to be local.

Other approaches to simulate many-body physics, such as quantum Monte-Carlo simulations, use heuristic assumptions on the state characterising the system. Although convergence is not guaranteed, quantum Monte-Carlo simulations usually succeed when the system is characterised by a locally restricted Gibbs Ansatz. The notion of locality used in quantum Monte-Carlo algorithm consists in assuming that the Hamiltonian describing the system is local, and hence the corresponding Gibbs state is also local.

With the research presented in Ch. 2, we have contributed in connecting these two notions of locality. Our main result consists in proving that classical restrictions of generic MPSs are quasi-locally Gibbsian. The proof of this result has been divided in the following steps. First, we have shown that any probability distribution defined on a one-dimensional lattice with open boundary conditions is exponentially close to a local Gibbs distribution, if the CMI between any tripartition of the lattice decays rapidly in the width of the middle region. Then, the CMI of classical restrictions of injective MPSs is demonstrated to decay if the purity condition is fulfilled. Finally, we have shown that the purity condition is a generic property in a concrete probabilistic model.

Outlook

The first question that naturally arises concerning our research presented in Ch. 2 is whether the results obtained are also valid for tensor networks of higher dimensions. A generalisation of our results in the context of matrix product density operators [71] or continuous MPSs [72] would also be interesting.

Additionally, the connection that we have established between classical restrictions of MPSs and Gibbs states could provide new understanding and algorithm improvements in quantum simulation. For example, could this connection be used for a rigorous convergence proof of the Monte Carlo wave function method [73]?

Within Ch. 2 we have proved that the CMI decays exponentially if the purity condition is satisfied, but no concrete decay rate has been given. It would be desirable to have a better insight into the dependencies of the decay rate and, even more, to obtain a closed expression.

There are also open questions regarding the purity condition. We have shown that the purity condition is necessary and sufficient for the quantum CMI, but only a sufficient statement has been proved for the classical CMI. One could wonder, then, if the purity condition is also a necessary condition in the classical case or if a weaker condition which is sufficient and necessary exists. On another note, is it easy to check whether a given MPS satisfies the purity condition?

Finally, our proofs make extensive use of the theory of random matrix products, and thus we wonder if these tools could also be advantageous in other fields.

Minimising statistical errors in gate calibration

Summary

Statistics is an essential tool in experimental science. Either before an experiment via DOE or afterwards via statistical analysis, statistics can be used to improve the results of experiments.

DOE is of significant importance in quantum mechanics because responses of measurements are predicted only probabilistically. In other words, every measurement outcome is a random variable distributed according to a concrete probability distribution with an associated variance. Moreover, when an experiment extracts more than one measurement response, we need to consider random vectors with possibly correlated components in the statistical analysis. Carefully planning DOE allows for the global statistical error to be minimised.

Chapter 4 encloses the application of DOE on the calibration protocol called GSC [39], and, in particular, in the calibration of a perturbed CNOT gate. We have proposed a modification on the calibration protocol that implies having two more single-qubit rotations available and allowing for a sequence length of five gates instead of four. In return, these changes on the protocol reduce the statistical error of the calibration by a factor of 0.47 when perfect measurements are considered and by a factor of 0.45 for imperfect measurements.

Outlook

The research conducted in Ch. 2 has opened some questions. We have reduced the statistical error of GSC by finding a trade-off between numerical stability and uncertainty. Nevertheless, we do not theoretically understand why the settings proposed here give a smaller statistical error than the sequences proposed in Ref. [39].

During the statistical analysis, we have numerically observed that, in the case of perfect measurements, the minimal statistical error does not depend on some of the rotations forming the sequences. It would be useful to have more insights into this property and understand why the dependency is different for perfect and imperfect measurements.

Our optimisation protocol has only considered modifications on the single-qubit rotations. The settings of GSC, however, can also vary in its initial state and measurement. Including variation on them could be a research line for further investigations.

We have assumed single-qubit rotations to be calibrated. A follow-up project could consider self-consistent calibration, i.e., calibrating the CNOT gate and the single-qubit rotations required for this calibration. How precise should single-qubit rotations be so that our GSC version still reduces the statistical error despite the cost of the number of rotations and the increased sequence length?

In order to obtain the error parameters, we have solved an inverse problem where the number of equations was the same as the number of parameters. One could consider more settings in the GSC such that the problem is overdetermined. Statistical analysis could be then applied to the redundant information, which may eventually lead to an extra reduction in the statistical error.

Finally, an experimental implementation of the version of GSC proposed in Ch. 4 would be interesting follow-up project.

Acknowledgments

In one session with my psychologist, I described doing a PhD like being in a tsunami. Ok, maybe I was having a hard time and not seeing the whole picture, but although it has not always been like this, there have been moments where I felt sinking. If now I am writing the acknowledgements of my PhD thesis, so if I arrived at a safe haven, it has been with the help of many.

Johan, thanks. You have been an essential part of this journey. Either before the pandemic, turning around, taking a pen and writing in the middle of a blank page, or clicking the zoom button during pandemic times and exchanging the pen and the blank page for the mouse and the screen of your laptop. Both actions are so natural for you. Your dedication to students, group-mates, family and simply to any person around you is admirable. Thanks for helping me *surviving* this tsunami.

(Big) David, thanks for adopting me. Having the opportunity to work with you has been inspiring and motivating. I have appreciated your clear and practical guidance as well as your attentive and open-minded leadership. Moreover, I am grateful that you pushed me and convinced me to start a project that involved coding, as this made me discover its fun.

Thank you, Michael, for supervising my challenging first project. Your expertise in formulating research questions and new ideas has been fundamental.

Working in the quantum-information research group in Cologne has been a great experience. Not only have I learned from all of you about physics, but also about fellowship. Especially, many thanks to Mariela for taking care of all of us with patience, joy and, above all, warmth. You have made me feel that nothing can go wrong when you are around.

Many thanks as well to experimentalists in the Bluhm group in Aachen. Your feedback on the second part of the thesis has definitely enhanced the project.

An meine Freunde, a les meves amigues. Alícia i Sandra sou violetes a la meva barca, alçant les veles quan fa falta o celebrant el cel obert quan la mar és en calma. Miriam, you continuously teach me about life. Kilian and Raphael, thanks for sharing experiences (and for reading parts of my thesis!).

Querida señorita Birke, gracias de corazón por mostrarme que existen otras formas. Sin usted, la última frase de estos agradecimientos nunca hubiera sido posible.

Gràcies Papa per transmetre'm la passió per la ciència i el coneixement. Mama, gràcies per estar sempre a l'altra banda del telèfon o agafant un avió si fos necessari. Sou un exemple de coratge, valentia i dedicació. Xarma, Nano, Josef, Sara, imprescindibles. Minis, avui què voleu un conte o un poema? Gràcies per sempre mostrar entusiasme per desvirtualitzar-me. Us estimo.

Dr. Niklitas, vielen Dank. Gràcies for not giving up when I had already dropped out. Wir sind ein Team (de tres).

La última frase és per mi. Agraeixo la meva resiliència.

Bibliography

[1] P. W. Shor. "Polynomial-Time Algorithms for Prime Factorization and Discrete Logarithms on a Quantum Computer". In: *SIAM Journal on Computing* 26.5 (Oct. 1997), pp. 1484–1509.

[2] S. K. Liao. et al. "Satellite-to-ground quantum key distribution". In: *Nature* 549 (2017), pp. 43–47.

[3] D. P. DiVincenzo. "The Physical Implementation of Quantum Computation". In: *Fortschritte der Physik* 48.9-11 (Sept. 2000), pp. 771–783.

[4] N. Friis et al. "Observation of Entangled States of a Fully Controlled 20-Qubit System". In: *Phys. Rev. X* 8 (2 Apr. 2018), p. 021012.

[5] C. D. Bruzewicz, J. Chiaverini, R. McConnell, and J. M. Sage. "Trapped-ion quantum computing: Progress and challenges". In: *Applied Physics Reviews* 6.2 (2019), p. 021314.

[6] N. K. Bernardes et al. "High Resolution non-Markovianity in NMR". In: *Scientific Reports* 6 (Mar. 2016).

[7] Y. Wu et al. "A programmable two-qubit solid-state quantum processor under ambient conditions". In: *npj Quantum Information* 5 (Dec. 2019), p. 9.

[8] F. Arute et al. "Quantum Supremacy using a Programmable Superconducting Processor". In: *Nature* 574 (2019), pp. 505–510.

[9] H.-S. Zhong et al. "Quantum computational advantage using photons". In: *Science* 370.65-23 (2020), pp. 1460–1463.

[10] "Wikipedia. Observable Universe". `https://en.wikipedia.org/wiki/Observable_universe`. Accessed: 29.01.2022.

[11] J. Eisert, M. Cramer, and M. B. Plenio. "Colloquium: Area laws for the entanglement entropy". In: *Reviews of Modern Physics* 82.1 (Feb. 2010), pp. 277–306.

[12] M. B. Hastings. "Solving gapped Hamiltonians locally". In: *Physical Review B* 73.8 (Feb. 2006).

[13] M. M. Wolf, F. Verstraete, M. B. Hastings, and J. I. Cirac. "Area Laws in Quantum Systems: Mutual Information and Correlations". In: *Physical Review Letters* 100.7 (Feb. 2008).

[14] M. B. Hastings. "Entropy and entanglement in quantum ground states". In: *Phys. Rev. B* 76 (3 July 2007), p. 035114.

[15] I. Arad, A. Kitaev, Z. Landau, and U. Vazirani. "An area law and sub-exponential algorithm for 1D systems". arXiv: quant-ph/1301.1162. 2013.

[16] V. Vedral. "Mean-field approximations and multipartite thermal correlations". In: *New Journal of Physics* 6 (Feb. 2004), pp. 22–22.

[17] K. G. Wilson. "The renormalization group: Critical phenomena and the Kondo problem". In: *Rev. Mod. Phys.* 47 (4 Nov. 1975), pp. 773–840.

[18] F. Verstraete, V. Murg, and J. Cirac. "Matrix product states, projected entangled pair states, and variational renormalization group methods for quantum spin systems". In: *Advances in Physics* 57.2 (Mar. 2008), pp. 143–224.

[19] R. Orús. "A practical introduction to tensor networks: Matrix product states and projected entangled pair states". In: *Annals of Physics* 349 (Nov. 2014), pp. 117–158.

[20] D. Perez-Garcia, F. Verstraete, M. Wolf, and J. Cirac. "Matrix Product State Representations". In: *Quantum Information & Computation* 7 (July 2007), pp. 401–430.

[21] M. Fannes, B. Nachtergaele, and R. F. Werner. "Finitely correlated states on quantum spin chains". In: *Communications in Mathematical Physics* 144.3 (1992), pp. 443–490.

[22] U. Schollwöck. "The density-matrix renormalization group in the age of matrix product states". In: *Annals of Physics* 326.1 (Jan. 2011), pp. 96–192.

[23] M. B. Hastings. "Solving gapped Hamiltonians locally". In: *Physical Review B* 73.8 (Feb. 2006).

[24] M. Sanz Ruiz. "Tensor Networks in Condensed Matter". Dissertation. München: Technische Universität München, 2011.

[25] F. Verstraete and J. I. Cirac. "Matrix product states represent ground states faithfully". In: *Phys. Rev. B* 73 (9 Mar. 2006), p. 094423.

[26] N. Schuch and J. I. Cirac. "Matrix product state and mean-field solutions for one-dimensional systems can be found efficiently". In: *Phys. Rev. A* 82 (1 July 2010), p. 012314.

[27] Z. Landau, U. Vazirani, and T. Vidick. "A polynomial-time algorithm for the ground state of 1D gapped local Hamiltonians". arXiv: quant-ph/1307.5143. 2013.

[28] I. Affleck, T. G. Kennedy, E. H. Lieb, and H. Tasaki. "Valence bond ground states in isotropic quantum antiferromagnets". In: *Communications in Mathematical Physics* 115 (1988), pp. 477–528.

[29] F. G. S. L. Brandão and M. Horodecki. "Exponential Decay of Correlations Implies Area Law". In: *Communications in Mathematical Physics* 333.2 (Nov. 2014), pp. 761–798.

[30] M. Sanz, D. Perez-Garcia, M. M. Wolf, and J. I. Cirac. "A Quantum Version of Wielandt's Inequality". In: *IEEE Transactions on Information Theory* 56.9 (Oct. 2010), pp. 4668–4673.

[31] D. M. Greenberger, M. A. Horne, and A. Zeilinger. "Going Beyond Bell's Theorem". In: *Bell's Theorem, Quantum Theory and Conceptions of the Universe*. Ed. by M. Kafatos. Dordrecht: Springer Netherlands, 1989, pp. 69–72.

[32] W. Dür, G. Vidal, and J. I. Cirac. "Three qubits can be entangled in two inequivalent ways". In: *Physical Review A* 62.6 (Nov. 2000).

[33] I. Affleck, T. Kennedy, E. H. Lieb, and H. Tasaki. "Rigorous results on valence-bond ground states in antiferromagnets". In: *Phys. Rev. Lett.* 59 (7 Aug. 1987), pp. 799–802.

[34] Y. Aragonés-Soria, J. Åberg, C.-Y. Park, and M. J. Kastoryano. "Classical restrictions of generic matrix product states are quasi-locally Gibbsian". In: *Journal of Mathematical Physics* 62.9 (Oct. 2021), p. 093511.

[35] O. K. Kozlov. "Gibbs Description of a System of Random Variables". In: *Probl. Peredachi Inf.* 10.3 (1974). English translation: Problems of Information Transmission, 1974, **10**:3, 258–265, pp. 94–103.

[36] P. Bougerol. "Products of Random Matrices with Applications to Schrödinger Operators". Progress in Probability. Birkhäuser Boston, 2012.

[37] T. Benoist, M. Fraas, Y. Pautrat, and C. Pellegrini. "Invariant measure for quantum trajectories". In: *Prob. Theory and Related Fields* 174 (2019), pp. 307–334.

[38] H. Maassen and B. Kümmerer. "Purification of quantum trajectories". In: *Dynamics & Stochastics*. Ed. by D. Denteneer, F. d. Hollander, and E. Verbitskiy. Vol. Volume 48. Lecture Notes–Monograph Series. Beachwood, Ohio, USA: Institute of Mathematical Statistics, 2006, pp. 252–261.

[39] P. Cerfontaine, R. Otten, and H. Bluhm. "Self-Consistent Calibration of Quantum-Gate Sets". In: *Physical Review Applied* 13.4 (Apr. 2020).

[40] Y. Tong. "The Multivariate Normal Distribution". Springer, New York, NY, 1990.

[41] D. C. Montgomery. "Design and Analysis of Experiments". Hoboken, NJ, USA: John Wiley & Sons, Inc., 2006.

[42] D. Aharonov and M. Ben-Or. "Fault-Tolerant Quantum Computation with Constant Error". In: *Proceedings of the Twenty-Ninth Annual ACM Symposium on Theory of Computing*. STOC '97. El Paso, Texas, USA: Association for Computing Machinery, 1997, pp. 176–188.

[43] J. Preskill. "Reliable quantum computers". In: *Proceedings of the Royal Society of London. Series A: Mathematical, Physical and Engineering Sciences* 454.1969 (Jan. 1998), pp. 385–410.

[44] J. F. Poyatos, J. I. Cirac, and P. Zoller. "Complete Characterization of a Quantum Process: The Two-Bit Quantum Gate". In: *Phys. Rev. Lett.* 78 (2 Jan. 1997), pp. 390–393.

[45] S. T. Merkel et al. "Self-consistent quantum process tomography". In: *Physical Review A* 87.6 (June 2013).

[46] J. B. Altepeter et al. "Ancilla-Assisted Quantum Process Tomography". In: *Phys. Rev. Lett.* 90 (19 May 2003), p. 193601.

[47] G. M. D'Ariano, M. G. A. Paris, and M. F. Sacchi. "Quantum Tomography". arXiv: quant-ph/0302028. 2003.

[48] B. Lévi, C. C. López, J. Emerson, and D. G. Cory. "Efficient error characterization in quantum information processing". In: *Phys. Rev. A* 75 (2 Feb. 2007), p. 022314.

[49] E. Knill et al. "Randomized benchmarking of quantum gates". In: *Phys. Rev. A* 77 (1 Jan. 2008), p. 012307.

[50] E. Magesan, J. M. Gambetta, and J. Emerson. "Scalable and Robust Randomized Benchmarking of Quantum Processes". In: *Phys. Rev. Lett.* 106 (18 May 2011), p. 180504.

[51] E. Magesan, J. M. Gambetta, and J. Emerson. "Characterizing quantum gates via randomized benchmarking". In: *Phys. Rev. A* 85 (4 Apr. 2012), p. 042311.

[52] A. Carignan-Dugas, J. J. Wallman, and J. Emerson. "Characterizing universal gate sets via dihedral benchmarking". In: *Phys. Rev. A* 92 (6 Dec. 2015), p. 060302.

[53] J. J. Wallman, M. Barnhill, and J. Emerson. "Robust characterization of leakage errors". In: *New Journal of Physics* 18.4 (Apr. 2016), p. 043021.

[54] A. Carignan-Dugas, K. Boone, J. J. Wallman, and J. Emerson. "From randomized benchmarking experiments to gate-set circuit fidelity: how to interpret randomized benchmarking decay parameters". In: *New Journal of Physics* 20.9 (Oct. 2018), p. 092001.

[55] K. Boone, A. Carignan-Dugas, J. J. Wallman, and J. Emerson. "Randomized benchmarking under different gate sets". In: *Phys. Rev. A* 99 (3 Mar. 2019), p. 032329.

[56] C. Dankert, R. Cleve, J. Emerson, and E. Livine. "Exact and approximate unitary 2-designs and their application to fidelity estimation". In: *Phys. Rev. A* 80 (1 July 2009), p. 012304.

[57] J. Eisert et al. "Quantum certification and benchmarking". In: *Nature Reviews Physics* 2.7 (June 2020), pp. 382–390.

[58] M. Kliesch and I. Roth. "Theory of Quantum System Certification". In: *PRX Quantum* 2.1 (Jan. 2021).

[59] S. Kimmel et al. "Robust Extraction of Tomographic Information via Randomized Benchmarking". In: *Phys. Rev. X* 4 (1 Mar. 2014), p. 011050.

[60] Y. Gu, R. Mishra, B.-G. Englert, and H. K. Ng. "Randomized Linear Gate-Set Tomography". In: *PRX Quantum* 2 (3 Aug. 2021), p. 030328.

[61] R. Brieger, I. Roth, and M. Kliesch. "Compressive gate set tomography". arXiv: quant-ph/2112.05176. 2021.

[62] L. Ruppert, D. Virosztek, and K. Hangos. "Optimal parameter estimation of Pauli channels". In: *Journal of Physics A: Mathematical and Theoretical* 45.26 (June 2012), p. 265305.

[63] G. Ballo, K. M. Hangos, and D. Petz. "Convex Optimization-Based Parameter Estimation and Experiment Design for Pauli Channels". In: *IEEE Transactions on Automatic Control* 57.8 (2012), pp. 2056–2061.

[64] R. Kosut, I. A. Walmsley, and H. Rabitz. "Optimal experiment design for quantum state and process tomography and hamiltonian parameter estimation". arXiv: quant-ph/0411093. 2004.

[65] J. Suzuki. "Quantum-state estimation problem via optimal design of experiments". arXiv: quant-ph/2012.11949. 2020.

[66] J. Nunn et al. "Optimal experiment design for quantum state tomography: Fair, precise, and minimal tomography". English. In: *Physical Review A* 81.4 (Apr. 2010), p. 042109.

[67] R. Blume-Kohout et al. "Demonstration of qubit operations below a rigorous fault tolerance threshold with gate set tomography". In: *Nature Communications* 8.1 (Feb. 2017).

[68] S. G. Johnson. "NLopt nonlinear-optimization package". `https://nlopt.readthedocs.io/en/latest/`. [Online; accessed 28-December-2021].

[69] M. J. D. Powell. "The BOBYQA algorithm for bound constrained optimization without derivatives". Cambridge, England: Department of Applied Mathematics and Theoretical Physics, technical report, NA2009/06, 2009.

[70] Y. Aragonés-Soria. "Minimising the statistical error in the calibration of quantum-gate sets". `https://github.com/yaiza-aragonessoria/min_stat_error_GSC.git`. 2022.

[71] F. Verstraete, J. J. García-Ripoll, and J. I. Cirac. "Matrix Product Density Operators: Simulation of Finite-Temperature and Dissipative Systems". In: *Physical Review Letters* 93.20 (Nov. 2004).

[72] F. Verstraete and J. I. Cirac. "Continuous Matrix Product States for Quantum Fields". In: *Physical Review Letters* 104.19 (May 2010).

[73] J. Dalibard, Y. Castin, and K. Mølmer. "Wave-function approach to dissipative processes in quantum optics". In: *Phys. Rev. Lett.* 68 (5 Feb. 1992), pp. 580–583.

[74] M. A. Nielsen and I. L. Chuang. "Quantum Computation and Quantum Information: 10th Anniversary Edition". 10th. USA: Cambridge University Press, 2011.

[75] B. Zeng, X. Chen, D. Zhou, and X.-G. Wen. "Quantum Information Meets Quantum Matter". New York, United States: Springer-Verlag New York Inc., 2019.

[76] R. Orús. "A practical introduction to tensor networks: Matrix product states and projected entangled pair states". In: *Annals of Physics* 349 (Nov. 2014), pp. 117–158.

[77] R. D. Somma, S. Boixo, H. Barnum, and E. Knill. "Quantum Simulations of Classical Annealing Processes". In: *Phys. Rev. Lett.* 101 (13 Oct. 2008), p. 130504.

[78] M. Kieferová and N. Wiebe. "Tomography and generative training with quantum Boltzmann machines". In: *Phys. Rev. A* 96 (6 Dec. 2017), p. 062327.

[79] J. Biamonte et al. "Quantum machine learning". In: *Nature* 549.7671 (Oct. 2017), pp. 195–202.

[80] F. G. Brandao and K. M. Svore. "Quantum Speed-Ups for Solving Semidefinite Programs". In: *2017 IEEE 58th Annual Symposium on Foundations of Computer Science (FOCS)*. 2017, pp. 415–426.

[81] J. Hammersley and D. Handscomb. "Monte Carlo Methods". Vol. 40. Methuen & Co, 1964.

[82] M. Suzuk. "Quantum Monte Carlo Methods in Equilibrium and Nonequilibrium Systems". Springer, Berlin, Heidelberg, 1986.

[83] H. De Raedt and W. von der Linden. "Quantum lattice problems". In: *Binder K. (eds) The Monte Carlo Method in Condensed Matter Physics. Topics in Applied Physics*. Vol. 71. Springer, Berlin, Heidelberg, 1992.

[84] A. N. Chowdhury, G. H. Low, and N. Wiebe. "A Variational Quantum Algorithm for Preparing Quantum Gibbs States". arXiv: quant-ph/2002.00055. 2020.

[85] N. Wiebe, A. Kapoor, and K. M. Svore. "Quantum Deep Learning". In: *Quantum Info. Comput.* 16.7–8 (May 2016), pp. 541–587.

[86] M.-H. Yung and A. Aspuru-Guzik. "A quantum–quantum Metropolis algorithm". In: *Proceedings of the National Academy of Sciences* 109.3 (2012), pp. 754–759.

[87] D. B. Kaplan, N. Klco, and A. Roggero. "Ground States via Spectral Combing on a Quantum Computer". arXiv: quant-ph/1709.08250. 2017.

[88] A. Riera, C. Gogolin, and J. Eisert. "Thermalization in Nature and on a Quantum Computer". In: *Phys. Rev. Lett.* 108 (8 Feb. 2012), p. 080402.

[89] M. Motta et al. "Determining eigenstates and thermal states on a quantum computer using quantum imaginary time evolution". In: *Nature Physics* 16.2 (Nov. 2019), pp. 205–210.